Response to reviewer #1

We thank the reviewer for the points raised. We made our best to account for her/his recommendations.

The reviewer's comments are in black and our answers are in red.
Modifications of the manuscript are reported in bold and italic.
The pages and lines reported here correspond to the original pdf.

The main aim of this paper is to evaluate the performance of the FIRR instrument under field campaign conditions. This is done successfully with overall performance shown to agree with laboratory performance within limitations imposed by the operational and environment conditions. Improving our understanding of the distribution and radiative effects of cirrus clouds in Arctic climates is highly important and TICFIRE a very worthwhile endeavour. Testing and improving the underlying technology for TICFIRE through the FIRR instrument is therefore crucial and this paper highly relevant.

Of the four main objectives mentioned at the end of the introduction I would suggest that the measurements described are not strictly a radiative closure experiment, the atmospheric state is not sufficiently well known to allow this. Similarly for the verification of the spectral signatures of cloud radiance. The work does assess the FIRR radiometric performance and demonstrates the sensitivity of FIRR measurements to atmospheric characteristics. The inclusion of the section on atmospheric cooling rates is not helpful for the objectives of the paper a fact emphasised by the lack of zenith view data. This can be omitted without impact on the paper. I would like more detailed information on the in-flight variability of the stabilitary data set, such as local humidity and ambient temperature, particularly at fixed flight levels. Please see additional text below.

We believe that the temperature and humidity measurements are sufficient to perform the radiative closure experiment in clear-sky conditions, given that many similar studies have called “radiative closure experiments” comparisons of radiance measurements to simulations fed by radiosoundings data, which is what is presented here. On the contrary, we fully agree that in cloudy conditions we do not have the necessary information to close the radiative experiment. We lack substantial information about cloud properties and the encountered clouds were too heterogeneous. This was already highlighted but is now stated more clearly.

We changed the introduction so that there is less confusion possible between the objectives of the campaign (which include radiative closure in all sky conditions) and those actually achieved. We also explicitly say that the radiative closure is completed for clear-sky conditions, while it is not for cloudy conditions.

p3 l.15 : “In the context of TICFIRE, ***there were four main reasons of*** flying the FIRR in the Arctic: “

p12 l.7 : “FIR simulations provide strong validation of the radiative transfer model, ***resulting in a satisfactory radiative closure for clear-sky conditions.***”

p22 l.13 : “further campaigns in the Arctic winter remain necessary, ***in particular to complete a radiative closure in cloudy conditions, which was not possible here due to lack of quantitative information about clouds properties.***”

p24 l.3 : “and their high heterogeineity. ***As a consequence, measured ice clouds spectral signature***

could not be compared to simulations with sufficiently well-constrained cloud properties. Such airborne campaigns"

As recommended by the reviewer, we removed the section of the discussion dedicated to the cooling rates, because it is mostly based on simulations contrary to the other results. Part of this section has been moved to the introduction to broaden the context of far-infrared radiation in the atmosphere and introduce the notion of efficient atmospheric cooling through LW emission of ice clouds.

Regarding the inflight variability of ancillary data, this is discussed in more details below.

Suggested changes to text:

Replace F-IR with FIR throughout text

done

Page2
line4: "host includes the strongly absorbing pure rotation band of water vapor" and coincides with a maximum in the water vapour continuum strength.

done

Line 8: "The emission maximum of Planck's function..."

done

Line 11: Reference to the Mars climate sounder is not relevant.

This reference has been removed from the introduction to be mentioned only in the presentation of the FIRR instrument, because of the similitude between both FIR filter radiometers. The same is true for the Diviner Lunar Radiometer.

P4 l.17: "***In this sense it is very similar to the Mars Climate Sounder (McCleese et al., 2007) and the Diviner Lunar Radiometer Experiment (Paige et al., 2010)***"

Line 32-33: This is a little confused, the wording may be clearer. "uttermost in Arctic regions because as discussed proportionately more energy is emitted from these colder surfaces at FIR wavelengths while the same time lower water vapour column increases atmospheric transmission.

done, with slight modifications.

Page 3
Line 22: vignetting by the chimney edges? I assume

Actually the edges of the chimney are not in the field of view. The vignetting simply corresponds to standard vignetting, that is the fact pixels on the edge of the illuminated area receive a bit less signal than those in the center.

"to avoid the ***small vignetting on the edges of the illuminated area.***"

Line 28: “One spectral measurement thus corresponds to a 0.8 s...”

done

Page 4:
There needs to be specific reference to the fact that the measurements are comprised from the average of all pixels in the 15 pixel diameter area illuminated by the scene footprint. The authors highlight the advantages of fast scanning and the high radiometric accuracy of their instrument but in the operational configuration described individual spectral band measurements are, if I understand the text correctly, off-set temporally and hence spatially. This should be made clear at this stage and placed in context to the along track averaging. The sequence described indicates 0.8 s averaging per band, 9 bands per filter wheel rotation totalling 7.2 s observation time for all bands. Given 3 scene views and 2 calibration scans per cycle that equates to 36 s. The Authors indicate that one complete sequence last 210 s, there is therefore some considerable time unaccounted for, can the Authors expand on this and explain the implications, if any, for high variability scenes such as that observed in the cirrus observations.

To insist on the fact that measurments correspond to spatial averages over the whole illuminated area, we slightly modified the text that was already quite explicit about this:

“In this study, the FIRR is not used as an imager, hence ***the data presented here correspond to averages over*** the selected area of 193 pixels”.

This is true, the acquisition of all channels is not simultaneous, hence consecutive measurements do not exactly correspond to the same scene. This is clearly stated now.

“for higher signal levels. ***Note, though, that measurements in successive spectral bands are offset temporally, hence spatially, which has to be borne in mind at the stage of data interpretation, especially when significant scene variations occur in less than 20 s.*** ”

As for the total duration, it can be roughly decomposed as follows:
- 0.8 * 10 * 5 = 40 s taking measurements on 10 filter wheel positions (a blank measurement is also taken)
- 1.5 * 17 * 5 = 126 s rotating the filter wheel (1.5 s to move of one position, total of 17 positions on the filter wheel)
- 3*15 s = 45 s rotating the pointing mirror

This means that a lot of time is lost rotating the filter wheel and the pointing mirror, which is one of the major issues that we should work on in the future.

This is now detailed:

“One FIRR measurement sequence lasts 210 s, ***during which approximately 40 s are used to actually take measurements and 170 s are spent rotating the filter wheel and the pointing mirror***. A sequence consists of [...]“.

“that measures all 9 filters ***in approximately 20 s***”

The impact of this temporal offset is already discussed in Fig. 4 that shows apparent spikes in

brightness temperatures.

The impact in the case of hight variability scenes is now detailed in the last section of the discussion dedicated to the recommendations for future operations:

p23 l.7 : "***It would also ensure that measurements in all channels are taken on the same target, which was not always the case during the campaign above leads or through highly heterogeneous ice clouds.*** Such ***technical*** developments"

Page 5:
Figure 1 does not add a lot to the text and can be omitted Table 1 would be more informative replaced with a spectral plot showing the filter transmission, similar to that of figure 2a in the Author's earlier paper, "A microbolometer-based far infrared radiometer to study thin ice clouds in the arctic".

We removed Figure 1 but moved the picture 1b to the paragraph describing the issue we had with the input of air inside the instrument, the latter being difficult to understand without the support of such a picture of the hatch. As suggested, we replaced Table 1 by the filters transmittance, indicating the band pass in the legend of the figure.

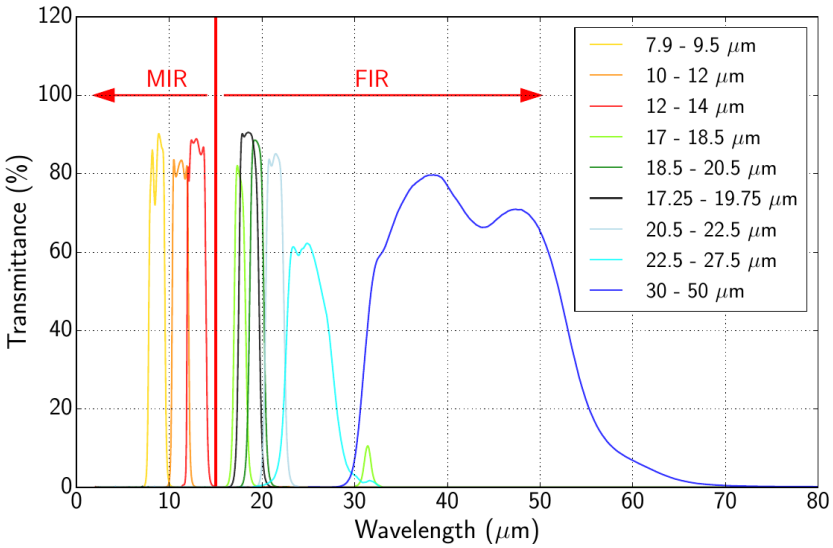

Page 6/7:
The description of the flight paths for the aircraft lacks detail, the longitudes indicated on figure 2 (left panel) are wrong (75/60/45 degrees being 15 degrees out). Choose one flight and expand to show detail of the profile track more clearly. Alternatively a more detailed figure of the flight path could be included with the case details.

The longitudes were updated because they were indeed 15 degrees off.
A detailed flight path for the 11 April flight has been added to Figure 2. It shows the size of the spirals and the trajectory typical for a vertical profile at constant speed. The color indicates the altitude.

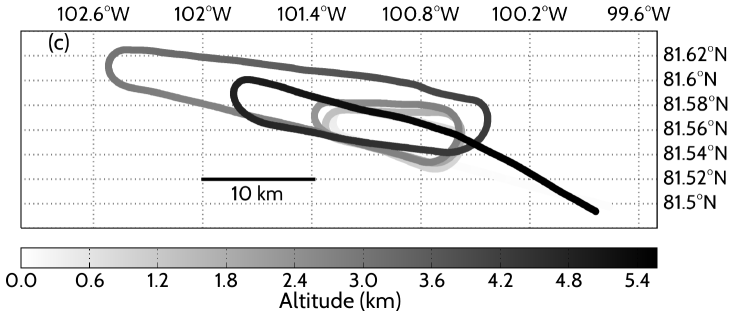

Page 8:
Line 6: Is the KT19 spectral response known and has this been applied derive surface temperature with the assumption of a spectrally flat surface emissivity of 0.995, be more explicit.

It was assumed that the KT19 measures the radiation in the range 9.6-11.5 µm (square response) and that in this range surface emissivty is flat at 0.995. This is now detailed.

P8 l.6 : "from the KT19 observations assuming a ***uniform spectral response of the instrument and a spectrally flat*** surface emissivity of 0.995 ***in the range 9.6-11.5 µm***."

Line 25-30:
How was the trend in ice temperature over the 30 minutes established, was this correlated against the KT19 data set for validation or was the KT19 data used to establish the trend?

This experiment was performed on snow when the aircraft was on the ground, so that only the FIRR was operating. The KT19 was not. Here we're interested in the resolution of the measurement, so that we removed the monotonic temporal trend attributed to snow temperature variation. This is now stated more clearly.

P8 l.28 : "for each spectral band. ***For all bands, the radiance increased continuously throughout the experiment, which was attributed to an increase of snow temperature. To remove this effect and focus on the resolution of the measurement only, the radiance series were first detrended,*** and the standard deviation of the residual was then computed."

Page 9:
Line3: "To further investigate the reduced thermal resolution observed..."

done

Line 21/22:
"the KT19 was -32.6C while a maximum of -24 C was observed in the atmospheric temperature profile between 1 and 2 km..."

done

Line 23: I do not believe you can justify suggesting no cloud above the aircraft from CALIPSO measurements made 3 hours previously, are there MODIS cloud cover products that are nearer in time that you can use.

This is true. An Aqua MODIS image was taken above the flight area at 6:45 PM (see images below), while the spiral ascent took place between 7:00 and 7:55 PM. This picture and the corresponding cloud products show a very large clear sky area around the flight area. The text was changing accordingly.

p7 l.2 : "***Images taken by the MODIS and the associated cloud products are also used to investigate cloud conditions above the aircraft***."

p9 l.23 : "and the ***Aqua MODIS image taken at 18:45 UTC shows*** that no clouds"

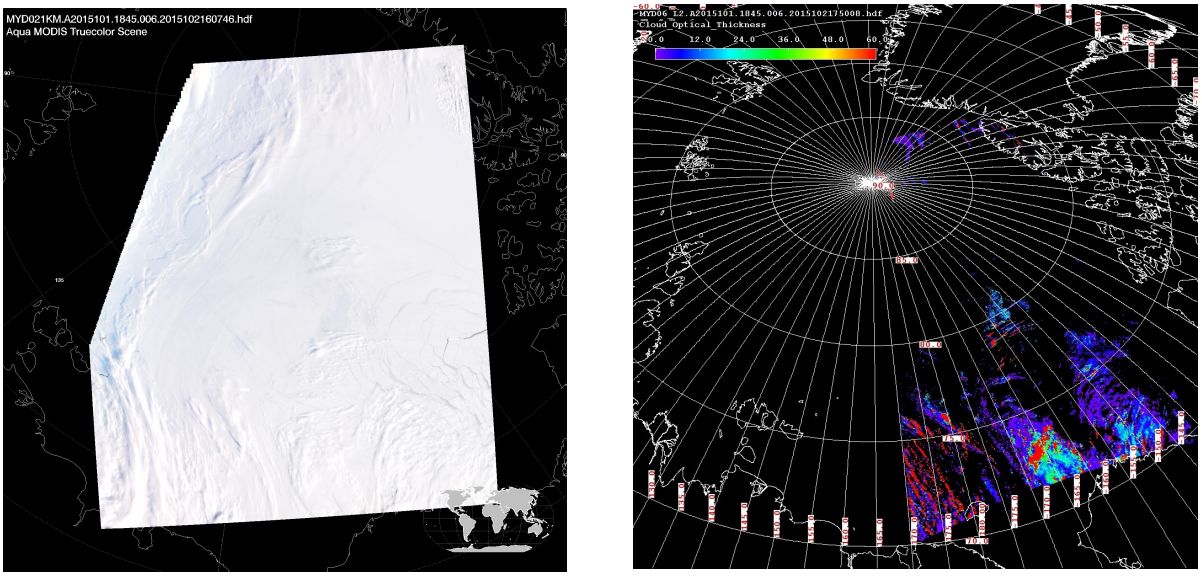

True color image (left) and cloud optical depth(right) from Aqua MODIS at 6:45 PM on 11 April

Line 25: A plot of the atmospheric transmittance vs altitude for each channel may help interpretation.

Following this suggestion the following figure was added. It shows the distance from the aircraft such that the atmospheric transmittance reaches 75%. It gives an idea of the distance to which each channel penetrates, which helps to interpret the radiance profiles shown in Fig. 4.

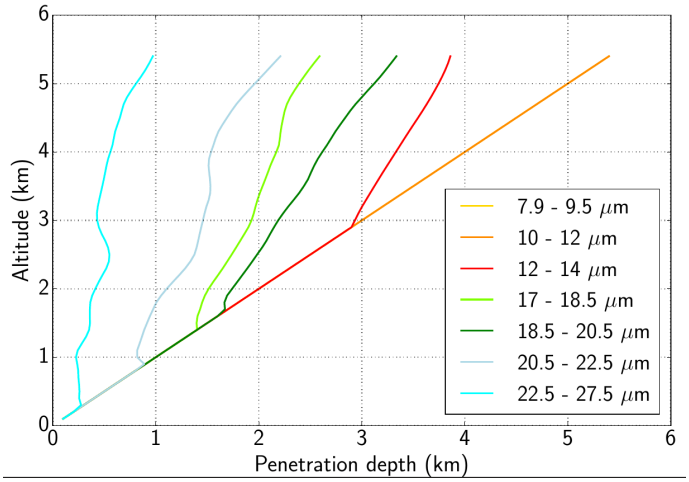

Some text was added accordingly:

p9 l.25 : "***To further illustrate this differential sensitivity to the temperature profile, Fig. 6 shows the penetration depth of each channel as a function of altitude. The channels that penetrate the least are sensitive to the conditions closest below the aircraft***."

Page 11:

Figure 4: 4c should indicate how the irradiance measurements were obtained.

"Vertical profiles of (a) temperature and relative humidity ***measured by in situ probes***, (b) FIRR brightness temperatures and (c) upwelling broadband LW irradiance ***measured by the CGR-4 pyrgeometer*** for 11 April flight."

Page 12:
Line 1: Be more specific about what feature you are referring to.

We clarified this:

p12 l.1 : "measurements show an unexpected ***peaked minimum***. Although the origin of ***this peak*** is not ***fully*** understood"

Fig 5. Can the Authors include error bars on the simulations using realistic uncertainties applied to the atmospheric data set used in the radiative transfer model.

Complementary simulations were performed for the 11 April flight, namely one with humidity increased by 2.5% and temperature increased by 0.3 K, the other with humidity decreased by 2.5% and temperature decreased by 0.3 K. These uncertainties correspond to the uncertainties of the temperature and humidy measurements. These simulations were used to estimate error bars in Fig. 5 (see below).

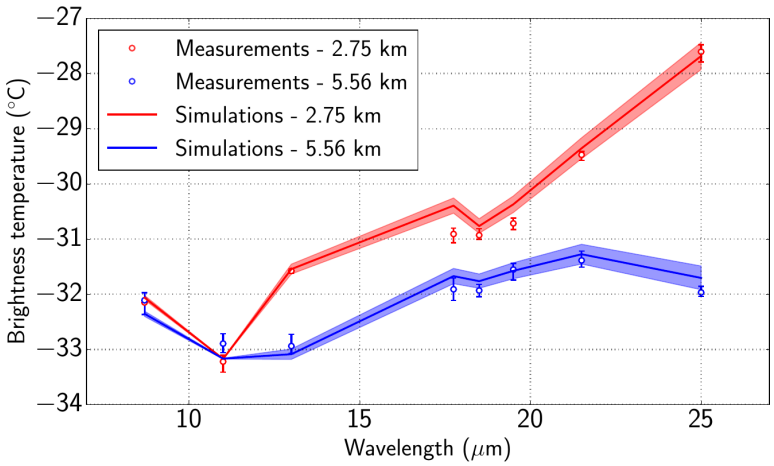

The text was also modified as follows:

p12 l.11 : "***In addition, most deviations between observations and simulations are within the range of uncertainties due to uncertainties of the temperature and relative humidity measurements.***"

Page 13:
Lines 19-34: It would be informative to see the spectrally resolved MODTRAN radiance output plotted as brightness temperature with the filter responses superposed, for the 11th, 20th and 21st April at the maximum aircraft altitude. Again uncertainties on the simulation BT's would be informative for figure 6.

The following figure was added to show the simulated high resolution brightness temperatures. The 21

April case is not shown because it is somehow redundant with the 20. The text was updated accordingly.

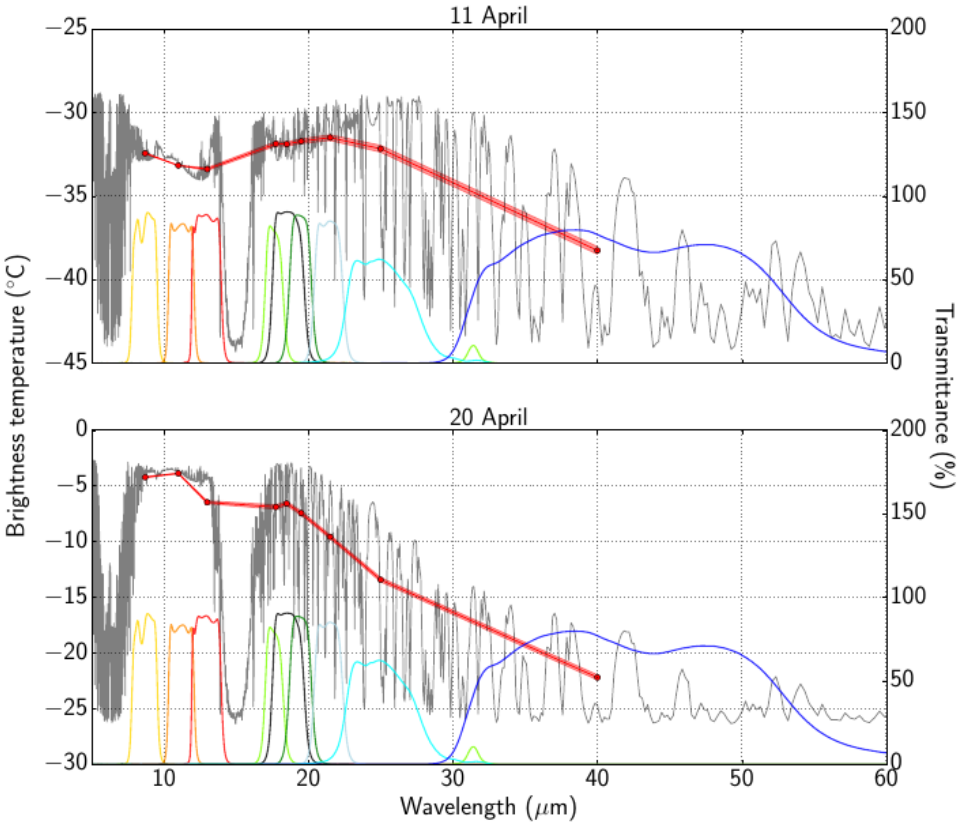

p13 l. 15 : "***The difference between the conditions encountered on 11 and 20 April is further illustrated in Fig. 9. It shows the high spectral resolution brightness temperature simulated by MODTRAN at 6 km altitude for both flights, and the corresponding simulated FIRR spectral signatures. This highlights the greater transparency of the atmosphere in the FIR for the 11 April***."

Page 15:
Figure 7 shows a 2-D image footprint for a 0.8 s scan, can the Authors include the relative positions for all 9 band observations along track for a single filter wheel rotation and indicate the position offsets between filter wheel cycles

We added some circles on the image to indicate when the first (plain line) and last (dashed) filters of a sequence are mesaured.

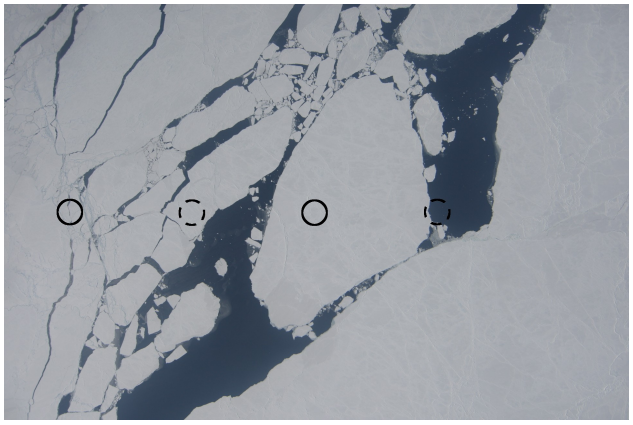

Line 3: “This question is left to future work...”

done

Line 5-6: You have no uncertainties placed on the MODTRAN simulations so stating the deficiencies here is not justified, for instance what is the along track variation in the measured humidity.

We show below the high temporal resolution measurements of water vapor, along with the “average” profile used for the MODTRAN simulation of 20 April. No significant variations of the water vapor are observed along track. The figure is not shown in the manuscript but this potential source of error is ruled out.

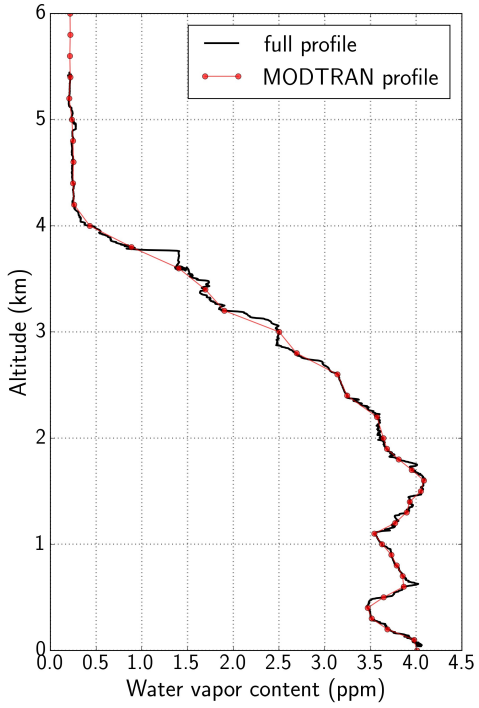

p13 l.32 : “***In addition, water vapor measurements along track did not show significant variability, so that spatial variability of water vapor can be ruled out. Only the incursion of a wet air mass below the aircraft before the end of the ascent could explain such a discrepancy between observations and simulations. In such case the water vapor profile used in the simulation would not correspond to the actual profile at the time of the measurement, but this is unlikely given that it was observed on two different flights***.”

Page 16:
Line 6: “, consistently with relatively large particles seen consistently by the 2D-C probe”

done

Page 18:
Line 15:
Inferences made from reference to figure 10 would be enhanced with inclusion of a linear plot of

relevant data sets as a function of aircraft altitude vs time (location). Colocated MODIS cloud optical depth/height can be superposed for reference.

The Figure 10 has been redrawn because the data shown were erroneously spatially interpolated. The new MODIS maps have been shifted by a few pixels, such that the interpretation is a bit changed in the manuscript.

Also, we added the timeseries of the brightness temperature difference, along with altitude and the time series of cloud optical depth and cloud top height corresponding to the maps shown in Fig. 10.

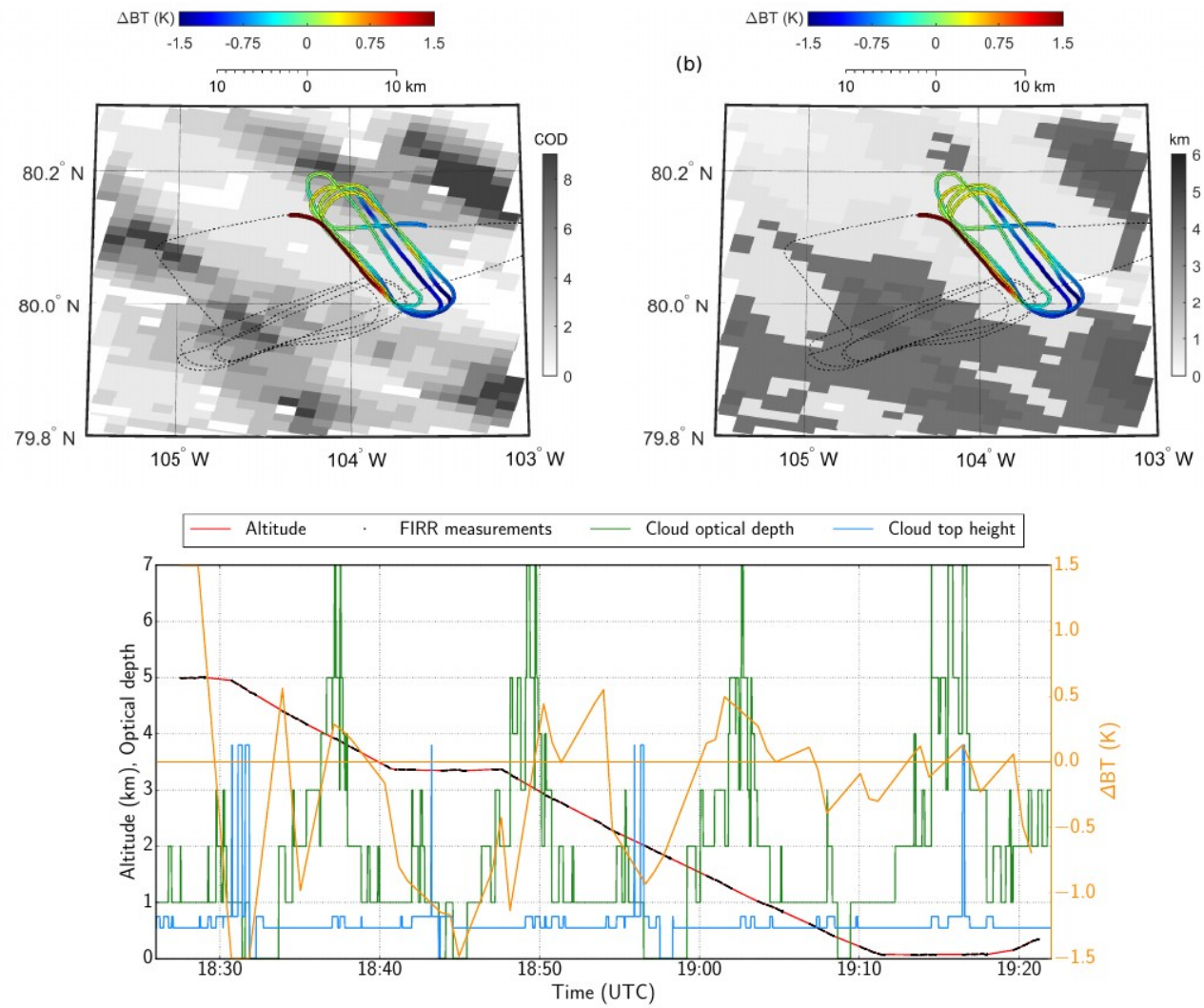

p18 l.14 : "In fact, the difference between the temperature measured by the 10- 12 μm channel and the simulation with τ = 2 (indicated by the color of the trajectory in Fig. 13) is minimum ***near the area corresponding to the high altitude cloud***, ***which suggests that the cloud there has an optical depth larger than 2***. It is higher elsewhere, meaning that FIRR senses warmer temperatures corresponding to either a thinner or lower cloud. ***The variations of the brightness temperature difference are more evident in Fig. 13c, that shows the time series of the difference along with the MODIS estimates of cloud characteristics.***"

Page 19:
Line 4: “making them somehow somewhat redundant.....”

done

Page 20.
Atmospheric cooling rates:
Mlynczak et al 2011, The INFLAME design is such that the net flux is measured directly thus allowing instantaneous cooling rates to be established. It is my understanding that FIRR would require combinations of sequential measurements of zenith and nadir views, similar spectrally resolved measurements of atmospheric cooling rates in the far-infrared have in fact been measured, Harries 2008.

The section of the discussion dedicated to the cooling rates has been removed. Part of this has been moved to the introduction and recommendations for future operations.

Line 10: “The net flux was computed from broadband sensors”. What sensors are these?
The inclusion of this section on cooling rates does not benefit the overall interpretation of the FIRR instrument performance. In itself it is not new nor does it expand on existing work. The “measured” broadband cooling rates are not detailed and the lack of FIRR zenith data is a hindrance. In my opinion this section should be omitted entirely.

The section has been omitted as suggested.

Page 22:
Line 1: “field of fiew view....”

done

Line 16: “instrument resolution” What aspect of instrument resolution are you referring to, spectral, spatial, thermal.

We added “***radiometric***”

Response to reviewer #2

We thank the reviewer for her/his relevant suggestions, that we tried to implement as much as possible.

The reviewer's comments are in black and our answers are in red.
Modifications of the manuscript are reported in bold and italic.
The pages and lines reported here correspond to the original pdf.

This paper describes the first field application of a far IR radiometer operated on-board the Polar 6 aircraft over Arctic regions during the NETCARE campaign. The paper shows the importance to measure the far IR spectral region and how much these measurements, acquired in all-sky conditions, can improve the sensitivity to specific humidity and the cooling rate of thin ice clouds.

General comment:
The paper is well written, clear in the description of the field campaign, and convincing in showing the importance to cover this observational gap in the spectral range of the IR emission. The data analysis is limited to few cases with few general implications for atmospheric science. However, considering that it belongs to the NETCARE special issue, I think that the paper is worth to be published in ACP and of general interest for the Earth radiation budget community.

Some changes are required to improve the figures and the description as indicated here below.

• Introduction. Some more references about the available measurements in Arctic should be added, e.g from ICECAPS experiment or the CANDAC network, in order to better stress the contribution of these new measurements.

The projects ICECAPS (at Summit) and CANDAC (at Eureka) are now mentioned, to insist that NETCARE contribution is mostly in terms of airborne measurements.

p3 l.4 : "***These scientific flights offered the possibility to probe the atmosphere in situ, thus providing a valuable complement to the extensive ground observations performed at well instrumented sites such as Summit (e.g. ICECAPS project, Shupe el al., 2013) and Eureka (e.g. CANDAC network, Mariani et al., 2012). Altogether, these initiatives aim at refining our understanding of the radiative budget of the Arctic and the critical role clouds play in it, in the continuity of the seminal Surface Heat Budget of the Arctic Ocean (SHEBA) program (e.g. Shupe et al., 2006)***."

• page 5 line 1. Does the same radiometric resolution apply to all the spectral bands ? If not, I would put the numbers in Tab.1 otherwise please clarify the text. Furthermore, is the radiometric resolution limited by the detector noise or by other reasons ? I would add some more information about the noise on the different channels and the related radiometric resolution, even if this is characterized in laboratory conditions.

The Table 1 has been removed and was replaced by a figure showing the spectral transmittances of each channel. The radiometric resolution is very similar from one band to another, because the absorptivity of the detector is spectrally flat (due to the gold black coating) and all filters have maximum transmittance around 80%. The resolution is a bit less, though, for the 22.5-27.5 and 30-50 channels which have slightly lower transmittances of the filter and of the package window, respectively. This is now detailed in the text. Regarding the resolution, in laboratory it is essentially limited by the detector noise.

p5 l.1 : “In this configuration, the radiometric resolution of the FIRR in laboratory conditions ***is essentially limited by detector noise and*** is about 0.015 W m^{-2} sr^{-1}***. This corresponds to noise equivalent temperature differences of 0.1 – 0.35 K for the range of temperatures investigated in this study. The resolution is nearly constant for the 7 bands ranging from 7.9 to 22.5 µm because the absorptivity of the gold black coating is spectrally uniform and the filters all have similar maximum transmittances. It is approximately 30% less for the filters 22.5 – 27.5 µm and 30 – 50 µm, because of limited filter transmittance for the band 22.5 – 27.5 µm and reduced package window transmittance for the band 30 - 50µm***.”

• page 6 line 2-4. It would be interesting to describe with more details the refinement introduced to better account for quick temperature variations. Otherwise this sentence is too general and not useful.

In Libois et al. (2016) the background radiance is assumed linear in time, and the rate is deduced using three measurements (ABB, HBB, next ABB). Here, another equation is added to the system, namely the next HBB measurement, so that we have 4 equations to retrieve 3 variables instead of 3 equations (eqs. 7 of Libois et al., 2016). Since it is a very technical detail and since the explanation would need too much reference to Libois et al. (2016), we decided to remove this detail.

p6 l.2 : “For previous flights, the calibration procedure detailed in Libois et al. (2016), that takes advantage of non illuminated pixels of the detector to remove the background signal, ensured good quality data for all bands except the 30 – 50 *µm*.“

• page 6 line 17-18. It is not clear whether the images were used or not. If not I would avoid to cite this probe.

The probe indicated the presence of large particles, which is used in the analysis, but the exact shape and size were not used because they were not reliable. It has been clarified.

P6 l.17 : “A PMS 2D-C imaging probe ***was supposed*** to detect larger particles, ***but*** the images were obscured due to a problem with the true air speed used in the image re-construction, preventing accurate retrieval of particle size distribution. ***Practically, this sensor was mostly used to assess the presence of large cloud particles, but did not provide quantitative information about particle shape or size.***”

• page 7 line 2. 5 cases are too few cases to provide a real overview of the Arctic conditions, they are an example of different conditions. Please rephrase the sentence.

“Overview” was replaced by “***samples***”

• page 8 sect. 3. Since this paper is published in ACP, even if it is mainly an instrumental paper, I would try to introduce since here the general scientific results expected in the framework of the NETCARE campaign in order to give more evidence to the peculiar results of this work within the general scientific problem of the special issue.

To present our results in the more general context of the NETCARE campaign, the objectives of the campaign are now presented in more details in Section 2.1. The general context was also recalled in the conclusion. However, we do not dwell too much on the original objectives, because due to the deficiencies in the cloud probe and to the lack of cloud cases, it is hard to derive from this campaign

general conclusions regarding the physics of ice clouds in the Arctic.

p4 l.7 : "***One of the objectives was to characterize at the same time the microphysical and the radiative properties of ice clouds, along with the nature of the aerosols, in order to further explore the conditions in which optically thin ice clouds form and how their microphysics depend on background aerosols.***."

p23 l.10 : "The first airborne campaign of the FIRR took place in the Arctic ***in the framework of the NETCARE aircraft campaign***. It was a great opportunity to study the ***radiative*** properties of the early spring Arctic atmosphere, ***and highlighted the importance of water vapor and ice clouds in this remote environment***."

• page 8 line 18. Please clarify whether the value of 0.015 W m-2 sr-1 applies to all the bands.

See above.

• page 8 line 25. This sentence is not completely clear because the calibration is not described. Furthermore, Sect 3.1 addresses the radiometric performance in terms of temperature resolution. It would be also interesting to have an idea of the absolute error of the measurement.

This sentenced has been removed because it was confusing. At the same time the description of the BB in Section 2.2.1 has been further detailed. The absolute error is about 0.02 W m^{-2} sr^{-1} according to laboratory experiments.

p4 l.1.25 : "***These correspond to BB nominal temperatures in flight but some experiments were performed with different BB temperatures depending on the environmental constraints, , which is not problematic since the instrument's response is linear in this range of temperature***."

p8 l.17 : "The FIRR performances were investigated based on laboratory and ground-based experiments by Libois et al. (2016). ***They estimated a radiometric resolution around 0.015 W m-2 sr-1 and an absolute error of 0.02 W m-2 sr-1, again slightly dependent on the channel considered***.

• page 11 line 6. I would say a "close agreement" above 2 km, below the difference is always more than 0.6 W m-2.

Done. 0.6 W m-2 is now 0.35 W m-2.

• page 12 line 3-4. If the peak is not present on the way down, please show this case in the figure.

This has been added to the figure. Since the descent shows a peak in the opposite direction, it has been mentioned in the manuscript and strenghtens the temperature adjustment hypothesis.

p12 l.3 : "This hypothesis is supported by the fact that data taken on the way down just before starting the ascent ***show a peak in the opposite direction***."

• page 11 fig. 4. In panel (b) the x-axis label should be Brightness temperature. I would also remove the temperature curve which is also shown in panel (a). Same for Fig. 6 panel (b) and (d).

Done, as well as for other figures showing vertical profiles of brightness temperature.

• page 13 line 10. Do you have some information about these clouds from CALIPSO ?

CALIPSO does not show any cloud above the aircraft altitude.

• page 13 line 17. In the comparison with simulation you should estimate the noise on measurements due to scene variations. Besides the aircraft movement considered here, please add some more considerations at least about the roll of the platform.

Scene variations do not result in an easily identifiable constant noise. Instead, it is mostly visible when strong variations occur, such as peaks seen on some vertical profiles. The roll of the platform is already meantione p11 l.2, but it is now converted in terms of distance.

p13 l.16 : “a single measurement of 0.8 s spanned 60 m at the surface. ***Similarly, a typical roll of 10° during the spiral corresponds to 1 km deviation at the surface when flying at 6 km.*** This could generate noise if the surface was not homogeneous at this scale, which was the case at the interface between the sea ice and open water.”

• page 13 line 26-27. The sentence "They are of little interest ..." is too general. This spectral range can be of great interest for satellite observations because you can see high altitude clouds.

This point has been detailed.

p13 l.25 : For this reason, the data in the 30 – 50 µm band are not reliable ***and are not shown in the rest of the paper. This is not critical in this study because at the flying altitude this band essentially probes local temperature. On the contrary it is expected to be very valuable from a satellite view, where it should provide information about water vapor and clouds at the very top of the troposphere.***”

• page 16 fig.8. As said before, I would use Brightness temperature for x-axis in panel (b) and show the temperature profile only in panel (a). Same for Fig.9.

Done.

• page 19 line 6. Since resolution was used for the radiometric measurement, the sentence is not clear. I would say: ... temperature variations of 0.2 K are detectable with a vertical resolution of ...

p19 l.6 : “***Given the radiometric resolution of the FIRR is about 0.2 K, temperature variations of 0.2 K are detectable with a vertical resolution of 100 to 200 hPa in FIR bands.***”

• General comment on figures. The font size of labels and scales in most of the figures should be enlarged to be clearer.

Done for all concerned figures

New references:

Shupe, M. D., Matrosov, S. Y., & Uttal, T. (2006). Arctic mixed-phase cloud properties derived from surface-based sensors at SHEBA. *Journal of the atmospheric sciences*, *63*(2), 697-711.

Shupe, M. D., Turner, D. D., Walden, V. P., Bennartz, R., Cadeddu, M. P., Castellani, B. B., ... & Neely III, R. R. (2013). High and dry: New observations of tropospheric and cloud properties above the Greenland Ice Sheet. *Bulletin of the American Meteorological Society*, *94*(2), 169-186.

Airborne observations of far-infrared upwelling radiance in the Arctic

Quentin Libois[1], Liviu Ivanescu[1,2], Jean-Pierre Blanchet[1], Hannes Schulz[3], Heiko Bozem[4], W. Richard Leaitch[5], Julia Burkart[6], Jonathan P. D. Abbatt[6], Andreas B. Herber[3], Amir A. Aliabadi[7], and Éric Girard[1]

[1]Department of Earth and Atmospheric Sciences, Université du Québec à Montréal, Montréal, Canada
[2]Centre d'applications et de recherches en télédétection (CARTEL), Université de Sherbrooke, Sherbrooke, Canada
[3]Alfred Wegener Institute, Helmholtz-Center for Polar and Marine Research, Bremerhaven, Germany
[4]Johannes Gutenberg University of Mainz, Institute for Atmospheric Physics, Mainz, Germany
[5]Environment and Climate Change Canada, Toronto, Canada
[6]Department of Chemistry, University of Toronto, Toronto, Canada
[7]Atmospheric Innovations Research (AIR) Laboratory, School of Engineering, University of Guelph, Guelph, Canada

Correspondence to: Quentin Libois (libois.quentin@uqam.ca)

Abstract. The first airborne measurements of the Far-InfraRed Radiometer (FIRR) were performed in April 2015 during the panarctic NETCARE campaign. Vertical profiles of spectral upwelling radiance in the range 8 - 50 μm were measured in clear and cloudy conditions from the surface up to 6 km. The clear-sky profiles highlight the strong dependence of radiative fluxes to the temperature inversion typical of the Arctic. Measurements acquired for total column water vapor from 1.5 to 10.5 mm also underline the sensitivity of the far-infrared greenhouse effect to specific humidity. The cloudy cases show that optically thin ice clouds increase the cooling rate of the atmosphere~~by a factor up to three~~, making them important pieces of the Arctic energy balance. One such cloud exhibited a very complex spatial structure, characterized by large horizontal heterogeneities at the kilometre-scale. This emphasizes the difficulty to obtain representative cloud observations with airborne measurements, but also points out how challenging it is to model polar clouds radiative effects. These radiance measurements were successfully compared to simulations, suggesting that state-of-the-art radiative transfer models are suited to study the cold and dry Arctic atmosphere. Although FIRR *in situ* performances compare well to its laboratory performances, complementary simulations show that upgrading the FIRR radiometric resolution would greatly increase its sensitivity to atmospheric and cloud properties. Improved instrument temperature stability in flight and expected technological progress should help meet this objective. The campaign overall highlights the potential for airborne far-infrared radiometry and constitutes a relevant reference for future similar studies dedicated to the Arctic, and for the development of spaceborne instruments.

1 Introduction

Since the early days of weather satellites, remote sensing in the infrared (IR) has been used to study the vertical structure of the Earth atmosphere (e.g. Conrath et al., 1970). Most instruments currently deployed, such as the Moderate Resolution Imaging Spectroradiometer (MODIS, King et al., 2003), the Atmospheric Infrared Sounder (AIRS, Aumann et al., 2003), and the

Infrared Atmospheric Sounding Interferometer (IASI, Blumstein et al., 2004), do not measure atmospheric radiation beyond approximately 15 μm, though, because sensing far-infrared radiation (~~F-IR~~FIR, 15 μm $< \lambda <$ 100 μm) generally requires a different technology (Mlynczak et al., 2006). However, probing the atmosphere in the ~~F-IR~~ FIR could provide valuable information and complement current observations. The ~~F-IR range hosts the purely rotational bands~~ FIR range includes the strongly absorbing pure rotation band of water vapor ~~. It is also where~~ and coincides with a maximum in the water vapor continuum ~~is strongest~~ strength (Shine et al., 2012). As such, it is especially promising for remote sensing of water vapor in the coldest regions of the atmosphere, that is the upper troposphere and the stratosphere (Rizzi et al., 2002; Shahabadi and Huang, 2014), and the polar regions in general (Turner and Mlawer, 2010; Blanchet et al., 2011; Palchetti et al., 2015). The ~~maximum of the~~ emission maximum of Planck's function shifts towards the ~~F-IR~~ FIR with decreasing temperature, so that increasingly more energy is emitted from this spectral region (Merrelli and Turner, 2012) compared to the more widely used 6.7 μm vibrational-rotational band (Susskind et al., 2003). Hence in cold atmospheres more than half of the radiation is lost to space from the ~~F-IR~~ FIR domain (Clough et al., 1992). ~~This is one of the reasons why the Mars Climate Sounder (McCleese et al., 2007) and the Diviner Lunar Radiometer Experiment (Paige et al., 2010) measure F-IR to probe the very cold atmosphere of Mars and the moon surface, respectively. The F-IR~~ The FIR signature of clouds also carries much information about cloud phase, optical thickness, particle ~~size distribution~~ effective size and particle shape for ice clouds (Rathke, 2002; Yang, 2003; Baran, 2007). This assessed sensitivity has recently stimulated the development of retrieval algorithms for ice cloud properties ~~(e.g. Blanchard et al., 2009)~~ (e.g. Blanchard et al., 2009; Palchetti et al., 2016) . Observing long term changes in the ~~F-IR~~ FIR emission of Earth could eventually provide valuable insight into the physical processes underlying climate change (Huang et al., 2010).

As a consequence, in the last three decades a number of scientific teams have demonstrated the need for improved observation of the Earth in the ~~F-IR~~ FIR (e.g. Mlynczak et al., 2002; Harries et al., 2008). In the meantime, several ~~F-IR~~ FIR spectrometers were developed. The Atmospheric Emitted Radiance Interferometer (AERI, Knuteson et al., 2004) has been extensively used for atmospheric profiling and cloud remote sensing (Turner and Löhnert, 2014; Cox et al., 2014). The Far-InfraRed Spectroscopy of the Troposphere (FIRST, Mlynczak et al., 2006) and the Radiation Explorer in the Far-InfraRed-Prototype for Applications and Development (REFIR-PAD, Palchetti et al., 2006) were developed within the framework of the satellite projects Climate Absolute Radiance and Refractivity Observatory (CLARREO, Wielicki et al., 2013) and REFIR (Palchetti et al., 1999), respectively. These instruments primarily aim at better constraining the radiative budget of the atmosphere, and have been operated from gondola and from the ground (Bianchini et al., 2011; Mlynczak et al., 2016). The Tropospheric Airborne Fourier Transform Spectrometer (TAFTS, Canas et al., 1997) has been used to explore the radiative properties of water vapor (Green et al., 2012; Fox et al., 2015) and to investigate the radiative properties of cirrus clouds (Cox et al., 2010). So far, all these spectrometers have been extensively used to improve the parameterization of the water vapor absorption lines and continuum in the ~~F-IR~~ FIR (Delamere et al., 2010; Liuzzi et al., 2014), in order to refine radiative transfer codes (Mlawer et al., 2012) and climate simulations (Turner et al., 2012).

Further understanding the radiative properties of the atmosphere in the ~~F-IR~~ FIR is of uttermost ~~importance~~ in the Arctic because ~~atmospheric cooling essentially occurs in this spectral range~~ proportionately more energy is emitted from cold regions at FIR wavelengths while at the same time lower water vapour column increases atmospheric transmission (Clough et al., 1992). Although ~~F-IR~~ FIR spectrometers have been used from the ground in Alaska and Northern Canada (Mariani et al., 2012; Fox et al., 2015), we are not aware of any such airborne measurements in the Arctic. The panarctic NETCARE (Network on Climate and Aerosols: Addressing Key Uncertainties in Remote Canadian Environments, http://www.netcare-project.ca) aircraft campaign, that took place in April 2015, attempted to fill this gap. This four-week campaign ~~involved the two instrumented Basler BT-67 Polar 5 and Polar 6 aircraft (e.g. Ehrlich and Wendisch, 2015) and~~ investigated the radiative properties of the atmosphere in clear and cloudy conditions~~.~~, with a stress on aerosols. These scientific flights offered the possibility to probe the atmosphere *in situ*, thus providing a valuable complement to the extensive ground observations performed at well instrumented sites such as Summit (e.g. ICECAPS project, **?**) and Eureka (e.g. CANDAC network, Mariani et al., 2012) . Altogether, these initiatives aim at refining our understanding of the radiative budget of the Arctic and the critical role clouds play in it, in the continuity of the seminal Surface Heat Budget of the Arctic Ocean (SHEBA) program (e.g. **?**) .

While most reported airborne ~~F-IR~~ FIR observations consist of constant altitude flights, vertical profiles of spectral radiance are very instructive to understand the vertical structure of the energy budget of the atmosphere (Mlynczak et al., 2011). For this reason, most measurements taken with the Far-InfraRed Radiometer (FIRR, Libois et al., 2016) during the campaign consisted of vertical profiles of upwelling radiance from the surface up to about 6 km. The FIRR was developed as a technology demonstrator for the Thin Ice Clouds in Far-InfraRed Experiment (TICFIRE, Blanchet et al., 2011) satellite mission, whose primary focus is on the water cycle in the Arctic, and on ice clouds in particular. Like cirrus at mid-latitudes (Cox et al., 2010; Maestri et al., 2014), ice clouds encountered in the Arctic significantly affect the atmosphere radiative budget in the ~~F-IR~~FIR, especially because they can fill the whole troposphere (Grenier et al., 2009). In very dry conditions, they act as particularly efficient emitters that radiatively cool the atmosphere (Blanchet et al., 2011) . Unlike the tropics, such ice cloud layers occur at any altitude, from the ground to the stratosphere (polar stratospheric clouds). Their ~~impact~~ radiative effect depends on their physical properties (Maestri, 2003; Maestri et al., 2005) , but is also very dependent on moisture (Cox et al., 2015), making the interactions between water vapor and Arctic clouds particularly complex.

In the context of TICFIRE, there were four main reasons of flying the FIRR in the Arctic~~served four main objectives~~: 1) assessing the FIRR radiometric performances in airborne conditions meant to mimic as closely as possible satellite nadir observations; 2) validating radiative transfer simulations in the ~~F-IR~~ FIR for clear and cloudy Arctic conditions through radiative closure experiments; 3) verifying the spectral signature of clouds radiance *in situ*; 4) investigating the sensitivity of FIRR measurements to atmospheric characteristics and better understanding the radiative budget of the Arctic atmosphere. The FIRR measurements taken during the campaign are presented in Section 2, along with complementary observations relevant to the radiative properties of the Arctic atmosphere. Five case studies are then detailed in Section 3 and serve as a basis to assess FIRR performances in airborne conditions and explore its sensitivity to atmospheric conditions. The sensitivity to temperature, humidity and cloud properties is further investigated in Section 4 using radiative transfer simulations. ~~The impact of an~~

optically thin ice cloud on atmospheric cooling rates is also discussed. Based on this unique experience, recommendations are provided for future operations of instruments similar to the FIRR in such airborne campaigns.

2 Materials and methods

2.1 The NETCARE campaign

The panarctic PAMARCMIP/NETCARE campaign (hereinafter NETCARE campaign) comprises many collaborators including the following institutions: Alfred Wegener Institut (AWI), University of Toronto, Environment and Climate Change Canada (ECCC), and more parties listed under the website. The campaign, which involved the two instrumented Basler BT-67 Polar 5 and Polar 6 aircraft (e.g. Ehrlich and Wendisch, 2015) , started in Longyearbyen (Spitzbergen) on 5 April with one week delay due to harsh weather conditions, with a single . There, only one flight dedicated to calibration was performed. Then the aircraft flew across Station North (Greenland) and operated around Alert, Nunavut (Canada) from 7 to 9 April. Afterwards, they moved to Eureka, Nunavut (Canada) and stayed there until 17 April. They continued to Inuvik, Northwest Territories (Canada), where Polar 6 operated until 21 April, while Polar 5 headed towards Barrow (Alaska). No flights were performed with Polar 6 from 14 to 19 April, due to cloudy conditions at Eureka and technical problems with the aircraft. The two aircraft had different scientific objectives, with Polar 5 mostly dedicated to sea ice studies and Polar 6 to aerosol and cloud studies. In the following, only Polar 6 operations are detailed, which consist of 10 scientific flights, amounting to 50 hours of campaign flight time.

The NETCARE campaign aimed at better understanding aerosol transport into the Arctic in the early spring, and its influence on ice cloud formation. One of the objectives was to characterize at the same time the microphysical and radiative properties of ice clouds, along with the nature of the aerosols, in order to further explore the conditions in which optically thin ice clouds form and how their microphysics depend on background aerosols. Many instruments were installed aboard Polar 6, including basic meteorology and radiation sensors, cloud microphysics instrumentation, particle counters, trace gas monitors and instruments for monitoring aerosol composition (e.g. Leaitch et al., 2016). Each flight was planned based on forecasts of clouds and transported pollution as well as the location of the A-Train satellite constellation (Stephens et al., 2002). The atmosphere was generally probed vertically from the surface (∼50 m) to approximately 6000 m (or the other way round) in about 50 min. To this end, the aircraft followed quasi-spirals of diameter 10 km.

2.2 *In situ* observations

2.2.1 The Far-InfraRed Radiometer (FIRR)

The FIRR (Libois et al., 2016) uses a filter wheel to measure atmospheric radiation in 9 spectral bands ranging from 8 to 50 μm (Table ??). Fig. 1). In this sense it is very similar to the Mars Climate Sounder (McCleese et al., 2007) and the Diviner Lunar Radiometer Experiment (Paige et al., 2010) , which use uncooled thermal sensors to probe radiation in the FIR. The FIRR sensor is a 2-D array of uncooled microbolometers coated with gold black (Ngo Phong et al., 2015), and radiometric calibration is achieved with two reference blackbodies (BB) at different distinct temperatures. The latter consist of cavities

whose temperature and emissivity are well known, so that the radiance they emit is accurately estimated. During the NETCARE campaign, the FIRR was onboard Polar 6 and measured upwelling radiance directly through a 56 cm-long vertical chimney~~(Fig. 2a)~~. At the bottom of the chimney, a rolling door ~~opened during the flight~~ (Fig. 2~~b)~~) opened during the flight, but remained closed otherwise to prevent dust or blowing snow from entering the instrument. Although the FIRR has a nominal field of view of 6° corresponding to a 20 pixels diameter area on the sensor, here only a 15 pixel diameter area is used to avoid the small vignetting on the edges of the illuminated area. This corresponds to a field of view of 4.5°, which translates into a footprint of 7.8 m at a 100 m distance, and 470 m at 6000 m. Since the temperature aboard the unpressurized cabin quickly varied between approximately 0 and 15°C, the ambient blackbody (ABB) was maintained at 15°C, while the hot blackbody (HBB) was set to 45 or 50°C. These correspond to BB nominal temperatures in flight but some experiments were performed with different BB temperatures depending on the environmental constraints, which is not problematic since the instrument's response is linear in this range of temperature (Libois et al., 2016) . One FIRR measurement sequence lasts ~~3 min 30 sand~~ 210 s, during which approximately 40 s are used to actually take measurements and 170 s are spent rotating the filter wheel and the scene selection mirror. A sequence consists of two calibration sequences (one on the ABB and one on the HBB) followed by 3 scene sequences, each sequence corresponding to one complete rotation of the filter wheel that measures all 9 filters in approximately 40 s. For each spectral band, 100 frames are acquired at 120 Hz and then averaged to provide a single 2-D image. One spectral measurement thus corresponds to a 0.8 s long acquisition and no supplementary temporal average is performed, highlighting the potential for fast scanning compared to interferometers that usually require averaging over several spectra to achieve comparably high performances (e.g. Mlynczak et al., 2006). Such acquisition rate is essential when looking at heterogeneous or quickly moving targets, as is the case from an aircraft or satellite view. It is the main advantage of trading spectral resolution for higher signal levels. Note, though, that measurements in successive spectral bands are offset temporally, hence spatially, which has to be borne in mind at the stage of data interpretation. In this study, the FIRR is not used as an imager, hence the data ~~are also spatially averaged~~ presented here correspond to averages over the selected area of 193 pixels. In this configuration, the radiometric resolution of the FIRR in laboratory conditions is essentially limited by detector noise and is about 0.015 W m^{-2} sr^{-1}~~, which~~ . This corresponds to noise equivalent temperature differences of $0.1 - 0.35$ K for the range of temperatures investigated in this study. The radiometric resolution is nearly constant for the 7 bands ranging from 7.9 to 22.5 μm because the absorptivity of the gold black coating is spectrally uniform and the filters all have similar maximum transmittances. It is approximately 30% less for the filters $22.5 - 27.5$ μm and $30 - 50$ μm, because of limited filter transmittance for the band $22.5 - 27.5$ μm, and reduced package window transmittance for the band $30 - 50$ μm. Such performances compare well with similar airborne spectroradiometers (e.g. Emery et al., 2014) and satellite sensors (e.g. MODIS).

~~FIRR spectral bands.~~

A critical issue during the campaign was the temperature stability of the instrument in operation. Indeed, the first flights were characterized by excessively noisy measurements, especially in the $30 - 50$ μm channel. This noise was due to excessive air circulation within the chimney, cooling down very quickly the calibration enclosure and the filters. In particular, the metallic mesh filter $30 - 50$ μm has a very low thermal capacity and its temperature significantly changed in less than 1 s, making the

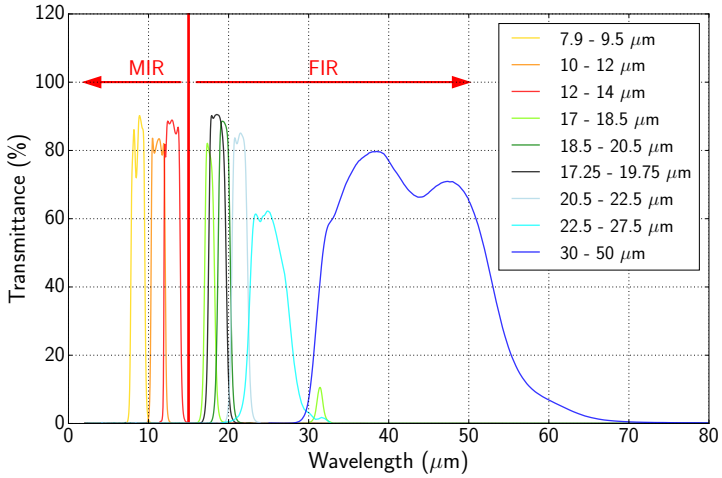

Figure 1. ~~(a) The FIRR setup aboard Polar 6. The optomechanical device is on~~ Spectral transmittances of the ~~floor while~~ nine filters of the ~~electronic components~~ FIRR, whose band pass are ~~above~~ indicated in the ~~insulated rack~~legend. Three filters cover the mid-infrared (~~b~~MIR) ~~The rolling door at the bottom of the chimney through which FIRR takes measurements. The door is shown~~ and six are in ~~optimal position for instrument stability, but nominal position is completely on the left. Flight direction is towards~~ the ~~left~~far-infrared (FIR).

Figure 2. The rolling door at the bottom of the chimney through which FIRR takes measurements. The door is shown in optimal position for instrument stability, but nominal position is completely on the left. Flight direction is towards the left.

acquired data unusable. A float-zone silicone window was available that could be placed at the entrance of the instrument, but we decided not to use it since its limited transmittance of 30% in the ~~F-IR~~ FIR drastically reduced signal level. This issue was fixed on 13 April by partially closing the rolling door in flight to prevent cold air flow from entering the inlet chimney, without impacting the field of view (Fig. 2). For previous flights, the calibration procedure detailed in Libois et al. (2016)~~was refined to better account for quick temperature variations. It~~ , that takes advantage of non illuminated pixels of the detector to remove the background signal, ~~and~~ ensured good quality data for all bands except the $30 - 50$ μm.

2.2.2 Other measurements

Polar 6 was equipped with a large set of sensors and instruments but only those relevant for the present study are mentioned below. Air temperature was recorded with an accuracy of 0.3 K by an AIMMS-20 manufactured by Aventech Research Inc. (Aliabadi et al., 2016). Trace gas H_2O measurement was based on infrared absorption using a LI-7200 enclosed CO_2/H_2O Analyzer from LI-COR Biosciences GmbH. In-situ calibrations during the flights were performed on a regular time interval of 15 to 30 min using a calibration gas with a known H_2O concentration close to zero. The uncertainty for the measurement of H_2O is 39.1 ppmv or 2.5 %, whichever is greater. Broadband longwave (LW) radiation was measured with Kipp & Zonen CGR-4 pyrgeometers installed below and above the aircraft (Ehrlich and Wendisch, 2015). These sensors have uncertainties of a few W m^{-2}. Nadir brightness temperature in the range $9.6 - 11.5$ μm was measured by a Heitronics KT19.85 II with a field of view of 2° and an accuracy of 0.5 K. A number of probes also provided qualitative information about the presence of cloud particles. Total and liquid water content were measured with a Nevzorov probe (Korolev et al., 1998). An FSSP-300 particle probe was used to measure particle size distributions from 0.3 to 20 μm from which cloud presence can be deduced (e.g. Ström et al., 2003). A PMS 2D-C imaging probe was ~~used~~ supposed to detect larger particles~~. However~~ , but the images were obscured due to a problem with the true air speed used in the image re-construction, preventing accurate retrieval of particle size distribution. Practically, this sensor was mostly used to assess the presence of large cloud particles, but did not provide quantitative information about particle shape or size. A sun-photometer specially designed for Polar 6 (SPTA model by Dr. Schulz & Partner GmbH) was mounted on top of the aircraft and continuously tracked direct solar radiation in 10 spectral bands in the range $360 - 1060$ nm. From these spectral measurements, the atmospheric optical depth was deduced and further processed with the SDA method (O'Neill et al., 2003) to retrieve the contributions of the fine (aerosols) and coarse (mainly cloud and precipitation) mode components. In addition to these particle measurements, black carbon concentration was estimated to give an indication on the level of pollution of the investigated air masses. To this end, ambient air was sampled with an inlet mounted above the cockpit of Polar 6, and a Single Particle Soot Photometer (SP2 by Droplet Measurement Technologies, Boulder, Colorado) was used to evaluate the mass of individual refractive black carbon particles per volume of air (Schwarz et al., 2006), from which the mass for particles within the size range $75 - 700$ nm was deduced. High resolution nadir pictures taken at 15 s intervals also provided valuable information about the surface and the presence of clouds.

2.3 Selected flights

For the present study, 5 vertical profiles taken during 5 different flights were selected. These flights, whose trajectories are shown in Fig. 3, were performed near Alert (82.5° N, 62.3° W), Eureka (80° N, 86.1° W) and Inuvik (68.3° N, 133.7° W) on 7, 11, 13, 20 and 21 April. All profiles were measured above snow-covered sea ice, which ensured that the surface was homogeneous contrary to flights performed above patches of snow and tundra or over areas of mixed sea ice and open water. All the investigated flights except 7 April were taken close to a track of the Cloud-Aerosol Lidar and Infrared Pathfinder Satellite Observations satellite (CALIPSO , Winker et al., 2003). Images taken by MODIS and the associated cloud products (Platnick et al., 2003) are also used to investigate cloud conditions above the aircraft. The 5 profiles were acquired in distinct

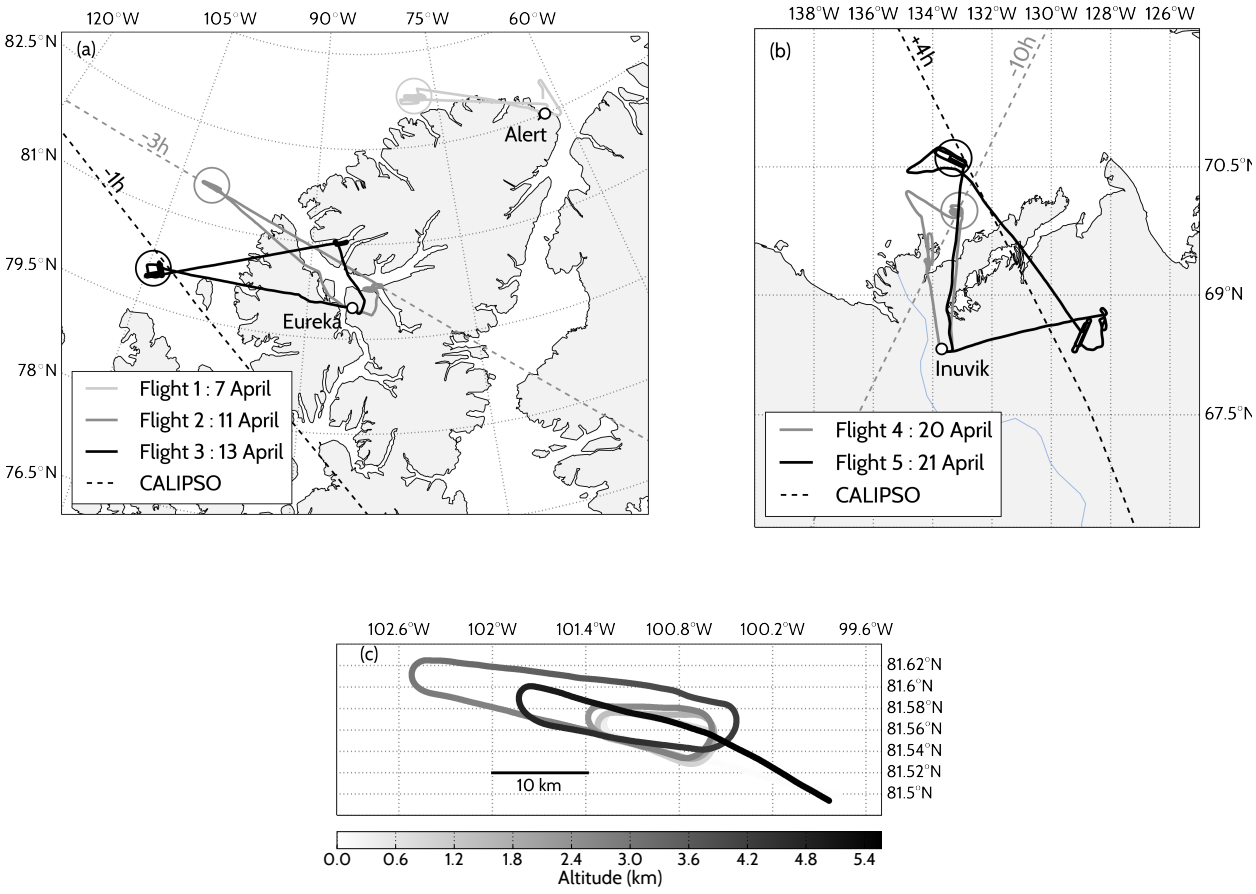

Figure 3. Selected flight trajectories around (~~left~~a) Eureka and (~~right~~b) Inuvik. The circles indicate where the detailed vertical profiles were performed. CALIPSO tracks are also shown and hours indicate how much earlier (-) or later (+) the satellite flew over. (c) Detailed spiral ascent for the 11 April flight.

atmospheric conditions, thus providing ~~a valuable overview~~ valuable samples of Arctic conditions in early spring. April 7 to 13 flights corresponded to typical conditions of the high Arctic cold season, with low temperatures and a pronounced inversion, while the conditions near Inuvik were more representative of subarctic spring, with near-melting temperatures at the surface and denser clouds typically found in the mid-latitudes. Some ice clouds were encountered on 7 April flight, but the more typical polar optically thin ice cloud was probed on 13 April near Eureka. The three other flights exhibited clear sky conditions below the aircraft.

2.4 Radiative transfer simulations

One objective of the study was to perform radiative closure experiments by comparing FIRR measurements with radiative transfer simulations based on thermodynamical and microphysical profiles recorded by the instruments aboard Polar 6. Here we used MODTRAN v.5.4 (Berk et al., 2005) to simulate upwelling radiance at flight level. MODTRAN uses absorption lines from HITRAN2013 and the MT-CKD 2.5 parameterization of the water vapor continuum (Clough et al., 2005) that proved reliable in the Arctic (Fox et al., 2015). The spectral surface emissivity of snow was taken from Feldman et al. (2014). Aerosols are approximated to the standard rural profile with a visibility of 23 km which is consistent with the presence of Arctic haze during the campaign. Multiple scattering is computed with DISORT (Stamnes et al., 1988) using 16 streams, and the band model is at 1 cm^{-1} spectral resolution. The model atmosphere has 75 levels from the surface to 30 km, with a resolution of 0.1 km near the surface stretching to 0.7 km at the top. In addition to radiances, MODTRAN was used to compute ~~atmospheric cooling rates (e.g. Clough et al., 1992) and~~ Jacobians through finite differences (Garand et al., 2001).

Temperature and humidity profiles were interpolated from the *in-situ* measurements up to the maximum flying altitude. Above, they were taken from the closest ERA-Interim reanalysis (Dee et al., 2011), the latter being offset to ensure vertical continuity. Ozone profiles for the whole column were also taken from ERA-Interim. Snow surface temperature was obtained from the KT19 observations assuming a uniform spectral response of the instrument and a spectrally flat surface emissivity of 0.995 in the range $9.6 - 11.5$ μm. All simulated clouds in this study are ice clouds defined by their optical thickness τ and ~~effective particle~~ particle effective diameter d_{eff}. Their single scattering properties are calculated after the parameterization of Yang et al. (2005) for cirrus clouds. Cloud geometrical characteristics were deduced from the combination of *in situ* observations. Optical thickness and effective cloud particle diameter were not directly measured. For 7 April, both quantities were tuned to minimize the deviation from measurements. For 13 April, the ~~effective particle~~ particle effective diameter was taken from DARDAR satellite product (Delanoë and Hogan, 2010) and simulations were performed for various optical depths.

3 Results

In this section, the FIRR radiometric performances are first analyzed based on experiments performed on the ground and during one flight. The five case studies are then analyzed in detail and the vertical profiles of radiance acquired in clear sky and cloudy conditions are compared to radiative transfer simulations.

3.1 FIRR radiometric performances in airborne configuration

The FIRR performances were investigated ~~based on~~ through laboratory and ground-based experiments by Libois et al. (2016)~~,~~ ~~who~~ . They estimated a radiometric resolution around 0.015 W m^{-2} sr^{-1} and an absolute error of 0.02 W m^{-2} sr^{-1}, again slightly dependent on the channel considered. In airborne configuration, the environmental conditions were more demanding due to cold ambient temperature and quick background temperature variations. The FIRR performances for this specific setup are thus estimated from two experiments for which the environmental conditions were similar to nominal airborne operation,

except the scene was more constant than in operation. Firstly, the brightness temperature of the snow surface below the aircraft was measured on Eureka runway on 12 April, while Polar 6 was parked without the propellers running. The ambient temperature was around -32°C, the ABB was at -9.5°C and the HBB at 20°C. Secondly, measurements taken on the closed rolling door just before landing on 11 April were analyzed. For this case, the ABB was at 15°C and the HBB at 45°C. ~~Although the BB temperatures were different than nominal values, this has no impact on the results since the instrument's response is highly linear and because the temperature difference between the HBB and ABB remained nearly constant.~~

The experiment on snow consisted of 10 consecutive measurement sequences covering 30 min, so that 30 radiances were recorded for each spectral band. ~~Those were first detrended to remove the effect~~ For all bands, the radiance increased continuously throughout the experiment, which was attributed to an increase of snow temperature~~variations over the period~~. To remove this effect and focus on the resolution of the measurement only, the radiance series were first detrended, and the standard deviation of the residual was then computed. The latter does not exceed 0.012 W m^{-2} sr^{-1}. The experiment performed on the rolling door consisted of 5 consecutive sequences, and the standard deviation of the signal was larger, reaching 0.021 W m^{-2} sr^{-1}. Figure 4a shows the corresponding brightness temperatures for both experiments, highlighting a temperature resolution around 0.1 K above snow and 0.2 K above the rolling door. Although the environmental conditions are slightly different in flight, these results provide a valuable reference and show that the installation of the instrument in the aircraft did not affect its performances.

To further investigate the reduced radiometric resolution observed in flight, Fig. 4b shows the sequence of brightness temperatures recorded on the rolling door. A recurrent pattern is observed within a sequence of 3 consecutive measurements, with the first temperature generally larger than the following ones. We interpret this as the signature of fast and complex temperature variations of the skin temperature of the ~~filter~~filters, that cannot be removed through the calibration procedure. We attempted to use the numerous temperature sensors embedded in the calibration enclosure and in the filter wheel to reconstruct the filters actual temperature, but this proved unsuccessful. Without any indication of whether any of the 3 consecutive points is the best, we simply conclude that this thermal instability results in an additive noise of approximate amplitude 0.2 K in worst conditions. This leaves room for future improvement of the instrument. The operational resolution of the FIRR nevertheless remains well below 0.5 K, which is still satisfactory and comparable to temperature measurements performed aboard Polar 6. This issue had not been noticed by Libois et al. (2016), most likely because in their study ambient temperature was closer to the internal temperature of the FIRR, limiting the range of filter temperature variations.

3.2 Clear sky cases

The profiles on 11, 20 and 21 April were all taken in clear sky conditions, but the total columns of water vapor were very different. These flights are specifically used to investigate the impact of temperature and humidity variations on the measured profiles of spectral radiances.

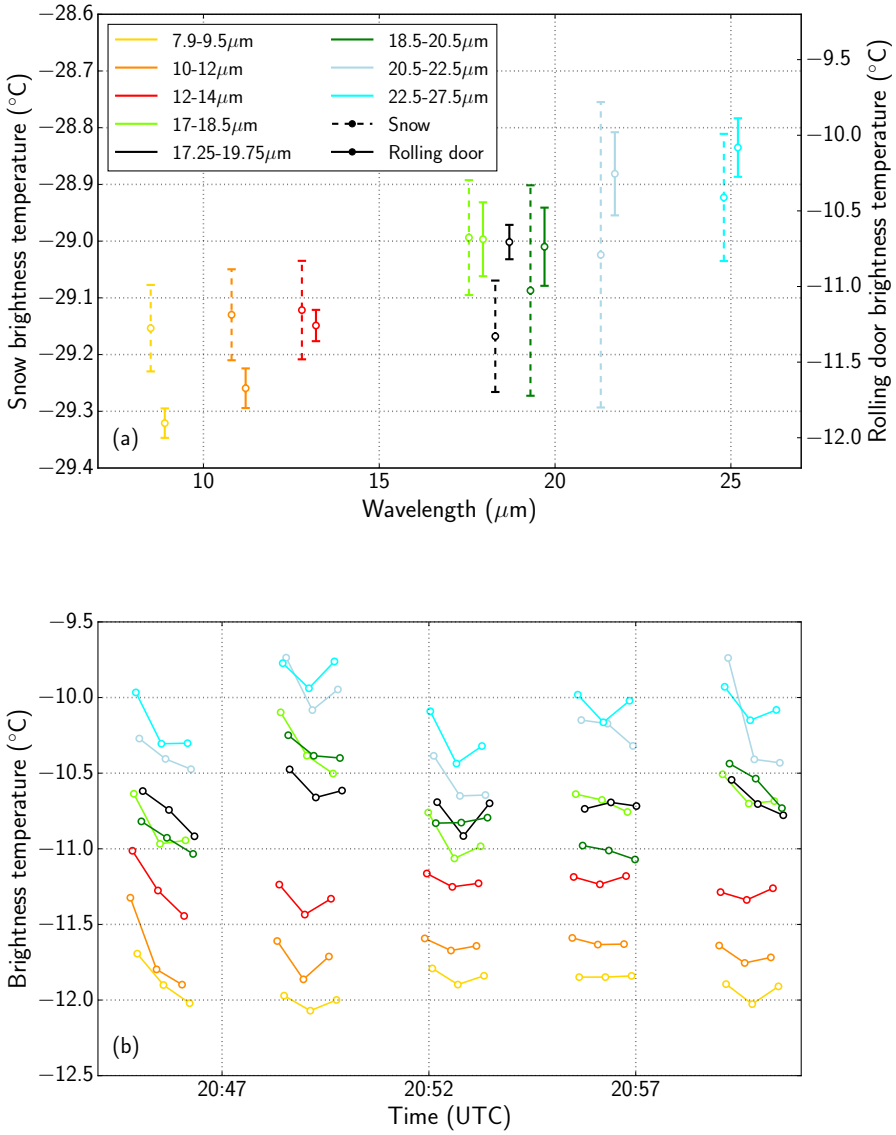

Figure 4. (a) Mean and standard deviations (error bars) of the detrended brightness temperatures along 10 sequences (i.e. 30 consecutive measurements) for measurements taken on snow on 12 April ($15:10-15:42$ UTC) and along 5 sequences on the rolling door on 11 April 11 ($21:45-22:00$ UTC). For 12 April, $T_{\mathrm{HBB}} = 20°\mathrm{C}$ and $T_{\mathrm{ABB}} = -9.5°\mathrm{C}$. For 11 April, $T_{\mathrm{HBB}} = 45°\mathrm{C}$ and $T_{\mathrm{ABB}} = 15°\mathrm{C}$. (b) Temporal evolution of brightness temperature for the 5 sequences acquired on the closed rolling door on 11 April. The $30-50$ μm band is not shown because it suffered from the temperature stability problem mentioned in Section 2.2.1.

3.2.1 11 April

The ascent started at 19:02 UTC and at 19:52 UTC Polar 6 reached the maximum altitude of 5.56 km, where it stayed for 4 min. On its way up it also levelled at 2.75 km for 7 min. The surface temperature retrieved from the KT19 was -32.6°C ~~and~~ while a maximum of -24°C was observed ~~from~~ in the atmospheric temperature profile between 1 to 2 km (Fig. 5a). The whole atmosphere was undersaturated with respect to ice, except near the surface. The total column water vapor was 1.5 mm, with 1.4 mm below 5.56 km. No clouds were observed and the ~~CALIPSO profile taken 3 hours earlier suggests~~ Aqua MODIS image taken at 18:45 UTC shows that no clouds were present above either. FIRR brightness temperature profiles show interesting features (Fig. 5b), with the temperature inversion more obvious for the longer wavelengths for which the atmosphere is more opaque. ~~The $17-18.5$ μm and $18.5-20.5$ μm profiles are very similar, implying relative redundancy between these two channels~~ To further illustrate this differential sensitivity to the temperature profile, Fig. 6 shows the penetration depth of each channel as a function of altitude. The channels that penetrate the least are sensitive to the conditions closest below the aircraft. As expected, the brightness temperature in the highly transparent atmospheric window ($10-12$ μm) is essentially constant with height since it is insensitive to the properties of the atmosphere. The slight increase of 0.5 K from the surface to the top is also observed in KT19 records and is probably the signature of surface temperature variations. The $17-18.5$ μm and $18.5-20.5$ μm profiles are very similar, implying relative redundancy between these two channels. The very distinct behaviors of window and ~~F-IR~~ FIR channels still result in nearly similar brightness temperatures at the top of the profile. This feature, typical of the Arctic, highlights the complexity of probing from space an atmosphere with a strong temperature inversion. The peaks in the shorter wavelengths channels around 4 km were found to visually correspond to variations of sea ice characteristics. They could be due to thinner and warmer sea ice or finer snow with higher emissivity (Chen et al., 2014). Since all individual measurements were used, the vertical resolution is close to 200 m. However, the instability along 3 measurements is noticeable, for e.g. the $18.5-20.5$ μm channel below 2 km. Besides this instrumental noise, part of the observed signal variation might be due to horizontal inhomogeneity, especially when the aircraft roll reaches up to 20° in turns.

The vertical profile of upwelling broadband LW radiation also highlights the temperature inversion, with a maximum around 2 km, similar to the ~~F-IR~~ FIR channels of the FIRR (Fig. 5c). LW fluxes have been simulated with MODTRAN and are also shown. The simulated and measured profiles are in ~~very~~ close agreement above ~~1~~2 km, with a root mean square deviation (RMSD) of ~~0.6~~0.35 W m^{-2}. Such a value is consistent with the accuracy provided by the manufacturer and the absolute uncertainty of 2 W m^{-2} suggested by Marty (2003) for such sensors. This is very satisfactory for a sensor sensitive only up to 42 μm while a significant part of the energy lies beyond, and considering that the calibration was done above 2°C. This agreement gives high confidence in the atmospheric profile measurements, but also in the aerosols modelled in MODTRAN, because errors in aerosol profiles could result in discrepancies of several W m^{-2} (Sauvage et al., 1999). Regarding the upper extrapolated part of the atmosphere, comparison of measured and simulated downwelling LW fluxes (not shown) are also in reasonably good agreement, which gives confidence in the ERA-Interim fields. Close to the surface, measurements show an unexpected ~~behavior~~peaked minimum. Although the origin of this ~~feature is not~~ peak is not fully understood, we believe this is an instrumental artifact resulting from the strong temperature gradient near the surface, and the sensor not being at thermal

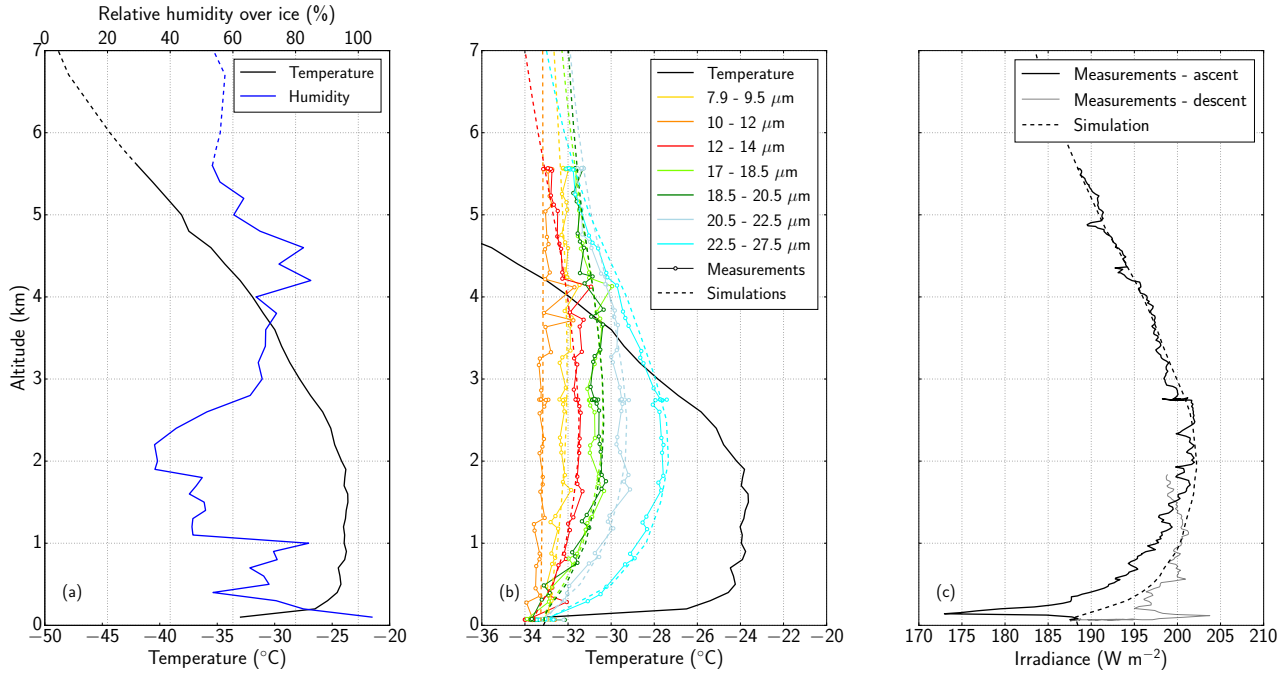

Figure 5. Vertical profiles of (a) temperature and relative humidity measured by in situ probes, (b) FIRR brightness temperatures and (c) upwelling broadband LW irradiance measured by the CGR-4 pyrgeometer for 11 April flight. The ascent portion correspond to the vertical profile and the descent portion shows the measurements taken 20 min prior to the ascent. The simulated FIRR brightness temperatures and LW irradiance are also shown. The $17.25 - 19.75$ μm band is not shown because it overlaps with others. The dashed lines in panel (a) correspond to the ERA-Interim profiles used for the simulations above maximum flying altitude.

equilibrium (Ehrlich and Wendisch, 2015). This hypothesis is supported by the fact that data taken on the way down just before starting the ascent ~~do not show the same feature~~show a peak in the opposite direction.

MODTRAN was also used to simulate FIRR brightness temperatures (Fig. 5b). The measured profiles for all channels are well simulated, with a mean bias and RMSD below 0.2 K. The agreement in the window bands confirms that no clouds were present below the aircraft. ~~F-IR~~ FIR simulations provide strong validation of the radiative transfer model, resulting in a satisfactory radiative closure in clear-sky conditions. The spectral brightness temperatures are compared at the two altitudes where multiple measurements were taken. Figure 7 shows the average measured brightness temperatures at 2.75 and 5.56 km, and the corresponding simulations. The spectral RMSD is below 0.15 K at both altitudes, which is very satisfying, given that MODTRAN user's manual suggests that the model accuracy is 1 K. The variability of the measurements at each step is below 0.4 K which is consistent with the results of Fig. 4b. In addition, most deviations between observations and simulations are within the range of uncertainties due to uncertainties of the temperature and relative humidity measurements.

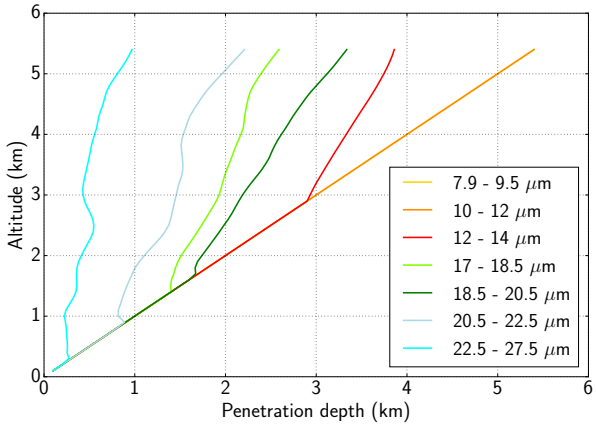

Figure 6. Penetration depth of each channel as a function of flying altitude for the 11 April flight. Penetration depth is defined as the downward distance from the plane such that the broadband transmittance in this channel reaches 75%.

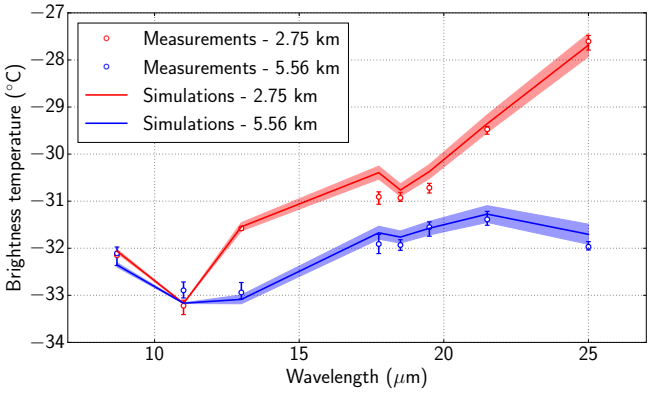

Figure 7. Measured and simulated spectral brightness temperatures at the two altitudes where Polar 6 levelled during 11 April flight. At both levels 4 consecutive measurements were taken. Their means and ranges are indicated by the circles and error bars, respectively. The shaded areas indicate the uncertainties in the simulations due to uncertainties on the measured temperature and relative humidity profiles, namely 0.3 K and 2.5%.

Overall, the simulations reproduce well the observations, which validates to some extent the radiative transfer code configuration and the implemented snow emissivity. However, such measurements can hardly be used for model improvement. As pointed out by Mlynczak et al. (2016), the inherent uncertainties related to the atmospheric measurements and radiative transfer parameterization likely exceed the FIRR measurements uncertainties. Agreement is thus satisfactory and encouraging for the performances of the instrument, but does not give further indications about the quality of the model inputs and parameterizations.

3.2.2 20 and 21 April

Both flights took place in the vicinity of Inuvik and showed relatively warm conditions and above freezing temperatures at the inversion level (~~Fig~~Figs. 8a and c). The cloud probes suggested that no clouds were present, which is consistent with the relative humidity profiles. For 20 April flight, a moist layer typical of long range transport was found, that peaked near 2.5 km at about 85% humidity with respect to water. Above 3.5 km, this layer was topped with drier air associated with weak air subsidence. Above 3.8 km, the air was very whitish, and the FSSP-300 and sun-photometer indicate increased level of aerosols. Likewise, SP2 measurements showed increasing amounts of black carbon with altitude, exceeding 0.1 μg m^{-3}, which is indicative of a polluted air mass. Similar conditions were encountered on 21 April, except that the polluted layer was located above 2.6 km, which again coincided with a drop of relative humidity. Sun-photometer data suggest the presence of high altitude clouds with optical depth around 0.2, but characterized by large variability. Those clouds were not accounted for in the simulations.

The vertical profiles of brightness temperatures are similar for both flights (Figs. 8b and d). Again, the window channels show very weak variations, which is characteristic of clear sky conditions. On the contrary, ~~F-IR~~ FIR channels are characterized by rapid variations near the surface and a larger lapse rate at higher altitude compared to the 11 April flight. These features are due to a sharper temperature inversion and a reduced transparency of the atmosphere (the column water vapor below 5.4 km are 10.3 mm and 10.5 mm, respectively). The difference between the conditions encountered on 11 and 20 April is further illustrated in Fig. 9. It shows the high spectral resolution brightness temperature simulated by MODTRAN at 6 km altitude for both flights, and the corresponding simulated FIRR spectral signatures. This highlights the greater transparency of the atmosphere in the FIR for the 11 April. The peak observed at 3.8 km on 21 April corresponds to measurements over open water, as shown by a picture taken concomitantly (Fig. 10). More generally, since Polar 6 approximately flew at 75 m s^{-1}, a single measurement of 0.8 s spanned 60 m at the surface~~, which~~. Similarly, a typical roll of 10° during the spiral corresponds to 1 km deviation at the surface when flying at 6 km. This could generate noise if the surface was not homogeneous at this scale~~. This~~, which was the case at the interface between the sea ice and open water.

The simulated brightness temperatures in the atmospheric window are in good agreement with observations, but deviations exceeding measurement uncertainties are found in the ~~F-IR~~ FIR channels for the upper part of the profile. The largest discrepancies are obtained in the $30-50$ μm band, with measurements being approximately 1.5 K warmer than the simulations. In fact, the air transmittance in this channel is so low that a significant part of the signal comes from the air contained in the 56 cm-long chimney just below the instrument, rather than from the atmosphere below. This artifact was noticed by Mlynczak et al. (2016). Using their correction (eq. 1), we find that air at -5°C and 50 % relative humidity in the chimney can increase the apparent brightness temperature at 5 km altitude by 1.5 K in the $30-50$ μm band, while the deviation does not exceed 0.3 K for the other channels. For this reason, the data in the $30-50$ μm band are not reliable ~~. They are of little interest because at low~~ and are not shown in the rest of the paper. This is not critical in this study because at the flying altitude this band essentially probes local temperature. ~~Consequently they are not shown in the rest of the paper~~On the contrary it is expected to be very valuable from a satellite view, where it should provide information about water vapor and clouds at the very top of the troposphere. The consistent positive bias of the simulations in the other ~~F-IR~~ FIR channels is more puzzling, especially because it is observed

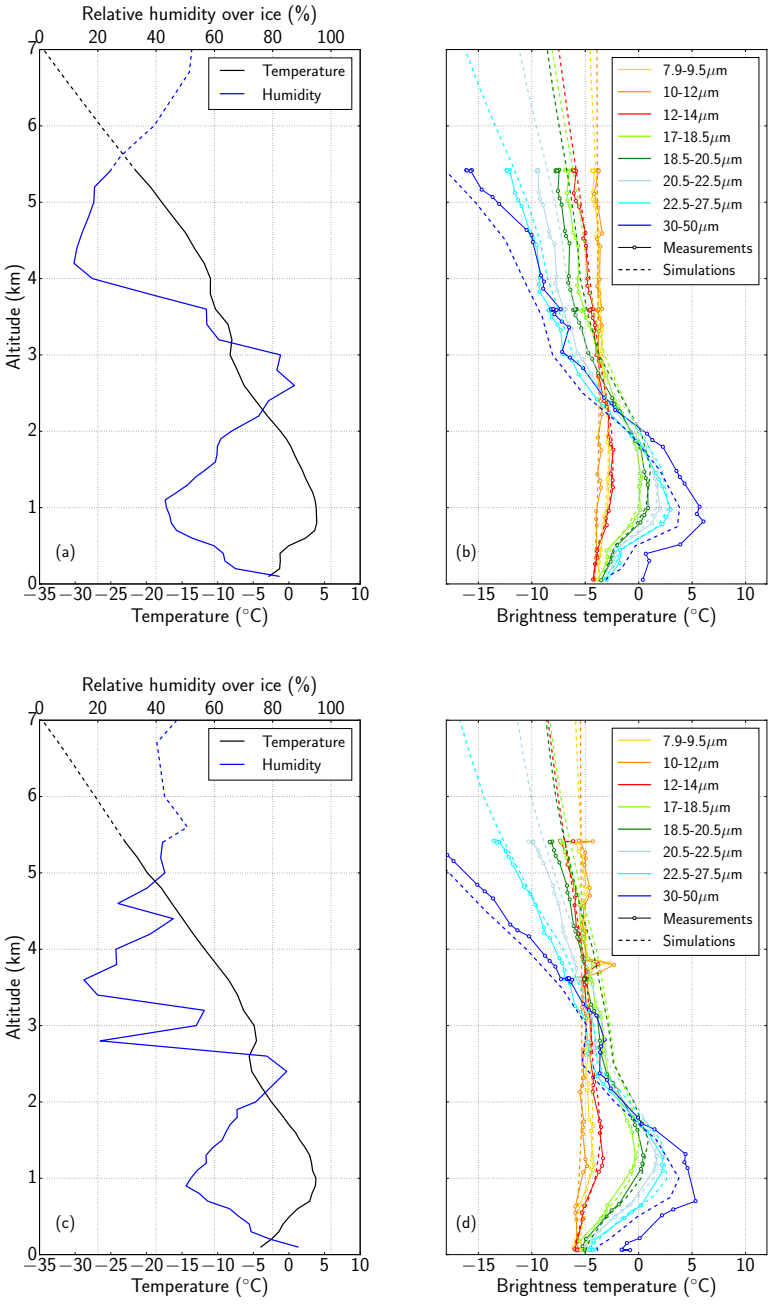

Figure 8. Vertical profiles of temperature and relative humidity for (a) 20 April and (c) 21 April flights. Measured and simulated FIRR brightness temperatures for (b) 20 April and (d) 21 April flights. The dashed lines in panels (a) and (c) correspond to the ERA-Interim profiles used for the simulations above maximum flying altitude.

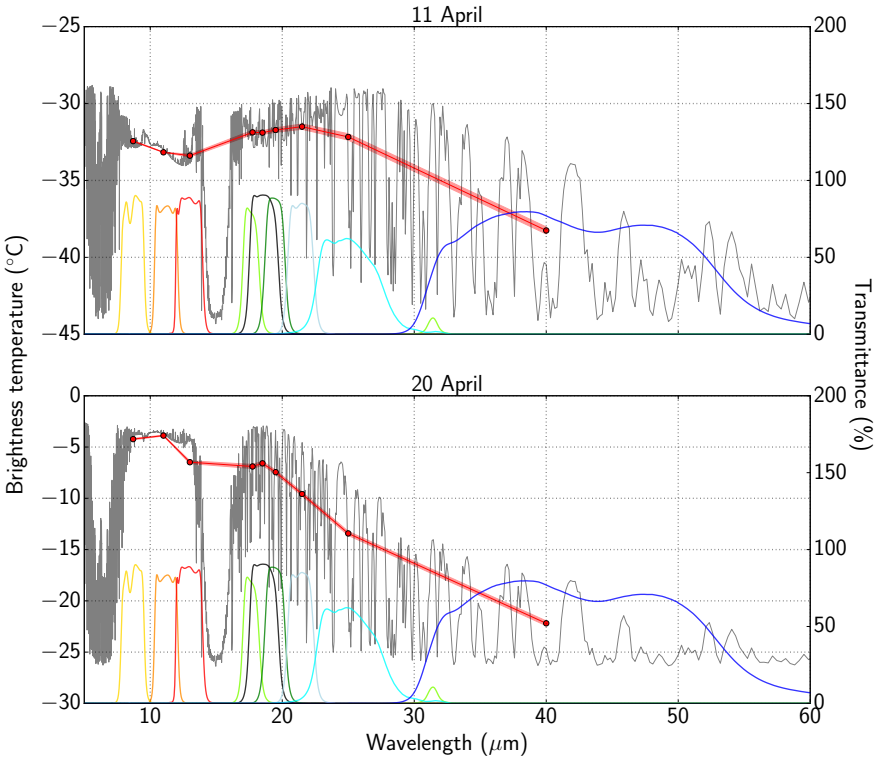

Figure 9. ~~Downward picture of~~ High spectral resolution brightness temperatures simulated with MODTRAN for the ~~surface taken on 21~~ 11 and 20 April flights at ~~17:35 UTC and 3.8~~6 km altitude. ~~The 300 m diameter circle depicts~~ FIRR filters transmittances are also shown, as well as the simulated FIRR ~~footprint at~~ spectral signatures. The red shaded areas indicate the ~~surface~~uncertainties in the simulations due to uncertainties on the measured temperature and relative humidity profiles.

in both flights. Several factors could explain such discrepancies. Inaccuracies in the water vapor continuum are ruled out because recent studies have shown uncertainties below 10% (Liuzzi et al., 2014; Fox et al., 2015), largely insufficient to explain such differences. Errors in water vapor measurements are also unlikely, because independent measurements taken by distinct instruments aboard Polar 6 show differences less than 20%, while only an increase larger than 50% could explain the observed differences. In addition, water vapor measurements along track did not show significant variability, so that spatial variability of water vapor can be ruled out. Only the incursion of a wet air mass below the aircraft before the end of the ascent could explain such a discrepancy between observations and simulations. In such case the water vapor profile used in the simulation would not correspond to the actual profile at the time of the measurement, but this is unlikely given that it was observed on two different flights. Adding an optically thin cloud between 6 and 9 km altitude did not improve the simulations either. Given the verified accuracy of the FIRR, we hypothesize that the differences are the consequence of the observed haze layer. This is in line with ~~with~~ the significant radiative signature in the IR shown by Ritter et al. (2005) for similar aerosol optical depths as those experienced in these two flights. The fact that the window channels are not impacted remains questioning, though.

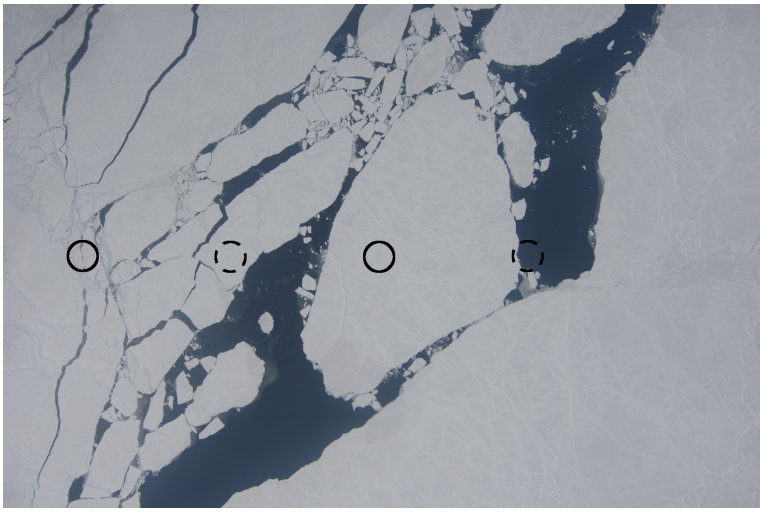

Figure 10. Downward picture of the surface taken on 21 April at 17:35 UTC and 3.8 km altitude. The 300 m diameter circles depict the FIRR footprint at the surface for a single 0.8 s measurement. Plain line circles indicate the relative positions of the aircraft when the measurement is performed on the first filter, and dashed circles when performed on the last filter (flight direction is to the right). It takes approximately 20 s to measure all nine filters, and another 20 s to come back to the position of the first filter.

This might be due to the specific nature of the wet aerosols forming the haze layer, which should have a signature similar to water vapor in the ~~F-IR~~FIR. This question is ~~let~~ left to future work, where hyperspectral measurements would certainly help investigating the detailed response. It should nevertheless be borne in mind that in these particular cases the greenhouse effect is underestimated in MODTRAN simulations, which can lead to significant deviations on the atmospheric and surface energy budgets.

3.3 Cloudy cases

Flights performed on 7 and 13 April are used to assess the radiative impact of optically thin ice clouds in the ~~F-IR~~FIR. They also highlight the difficulty to compare *in situ* observations to radiative transfer simulations due to high variability of the cloud microphysics.

3.3.1 7 April

During this flight west of Alert, singular atmospheric conditions were encountered. Near the surface, a saturated layer was found up to 1.1 km where a cloud was present, as detected by the Nevzorov and 2D-C probes. Another cloud was found above 4 km, that extended up to the maximum flying altitude of 6 km. In between, the atmosphere was very dry. The temperature profile had a complex signature near the surface, where a double temperature inversion was observed (Fig, 11), probably due to radiative cooling at top of the near-surface cloud. Observed FIRR brightness temperatures are consistent with the atmospheric

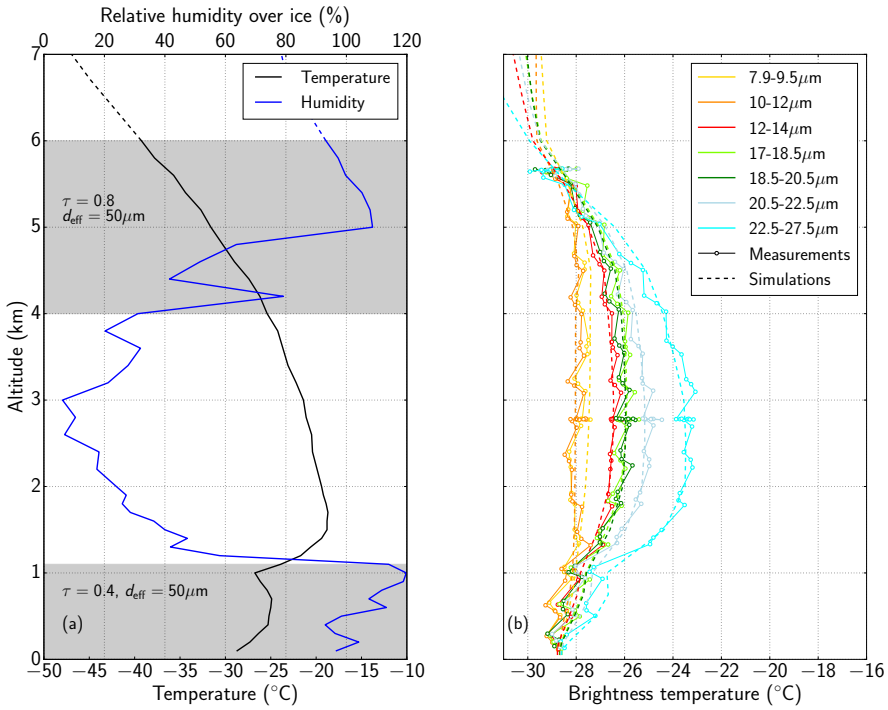

Figure 11. Vertical profiles of (a) temperature and relative humidity, and (b) measured and simulated FIRR brightness temperatures for 7 April flight. Shaded areas in panel (a) indicate the presence of clouds. The optical thickness and ~~effective~~ particle effective diameter used for the simulations are also indicated. The dashed lines correspond to the ERA-Interim profiles used for the simulations above maximum flying altitude.

profile. In the clear sky region, the profiles are similar to that of 11 April. In clouds, brightness temperature varies more rapidly with altitude, as a consequence of increased absorption and scattering in all channels. Consequently, all brightness temperatures samples at 5.7 km are contained in a narrow 1.5 K range.

Since CALIPSO does not cover such high latitudes, we do not have supplementary information regarding the clouds properties. The profile of relative humidity suggests that the cloud was initiated above 5 km in saturated air with respect to ice, and below ice particles were precipitating, without saturating the air. For the MODTRAN simulations, the ~~effective particle~~ particle effective diameter was set to 75 μm, ~~consistently~~ with relatively large particles consistently seen by the 2D-C probe, but missed by the FSSP-300. We then tuned the optical depth to 0.5 for the near-surface cloud layer and 1.0 for the upper layer cloud. This set of cloud properties produces brightness temperatures profiles in agreement with the measurements. The brightness temperature difference between $7.9 - 9.5$ μm and $10 - 12$ μm channels is larger in the model than in the observations yet, which suggests an imperfect definition of aerosol and haze profiles.

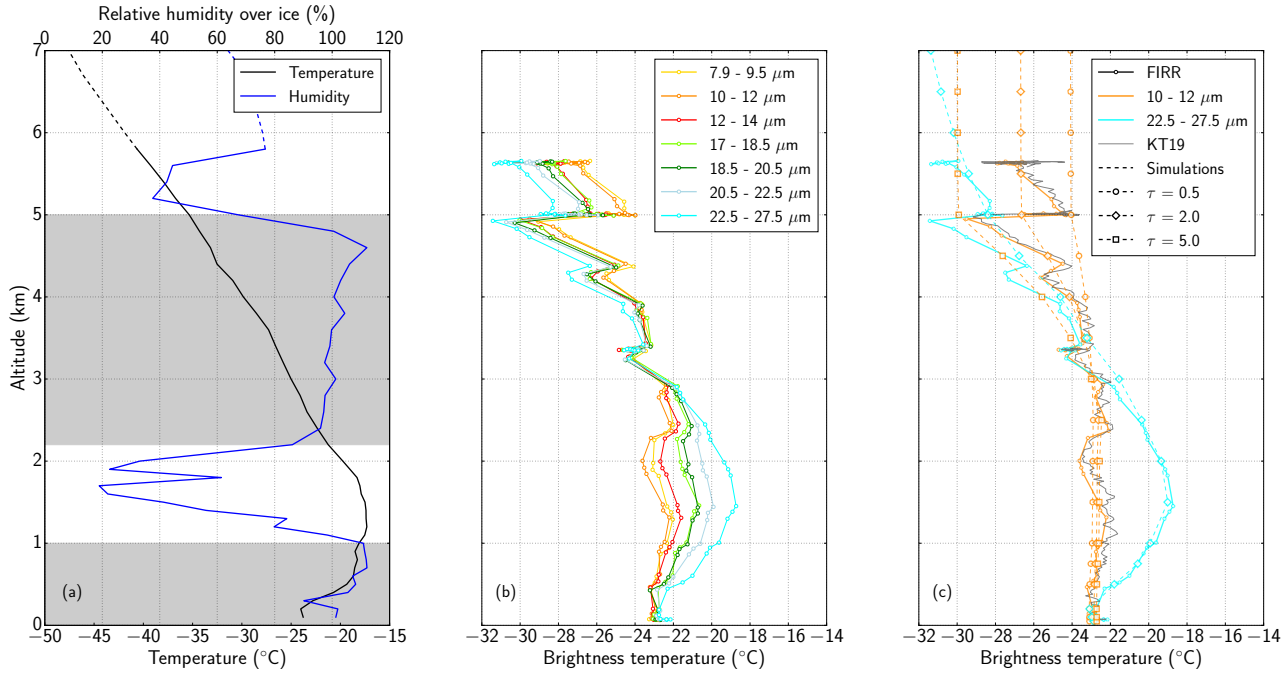

Figure 12. Vertical profiles of (a) temperature and relative humidity, and (b) FIRR brightness temperatures for 13 April flight. In panel (a), the shaded areas indicate the presence of clouds and the dashed lines correspond to the ERA-Interim profiles used for the simulations above maximum flying altitude.. Panel (c) shows measured and simulated brightness temperatures for two FIRR bands and various optical depths of the upper cloud. KT19 temperatures are shown as well for comparison to FIRR 10 - 12 μm channel.

3.3.2 13 April

The best case of optically thin ice cloud was observed during 13 April flight. A vertical profile was taken during the descent between 18:15 and 19:12 UTC. The temperature profile was fairly typical of Arctic winter conditions, with an inversion at 1.3 km and surface temperature around -25°C (Fig. 12a). A tenuous cloud layer was found below 1 km and a much thicker cloud was observed between 2.2 and 5 km according to the combination of 2D-C and FSSP-300 probes. These two instruments, along with the relative humidity profile, suggest that ice particles formed above 3 km but large precipitating crystals were observed down to 2.2 km. This cloud is similar to a TIC-2B type from the classification of Grenier et al. (2009). The FIRR brightness temperatures are characterized by high vertical variability, especially above 3 km (Fig.12b). This variability is identical for all bands, suggesting that it is due to actual scene variations. The excellent match between KT19 measurements and the $10-12$ μm channel confirms that observed variations are not instrumental artifacts (Fig. 12c). Instead, they are attributed to cloud horizontal variability. This hypothesis is supported by the sun-photometer data that show highly varying optical depth above the aircraft as well.

Since the aircraft is flying in quasi-spirals of 10 km diameter, any cloud variability below this scale results in signal variability on the vertical profile. Downlooking pictures taken on Polar 6 show that above 3 km, surface features were intermittently visible, meaning that cloud optical depth varied substantially along the flight path. Attempting to reproduce the measured brightness temperature profiles with a 1-D model was impractical. Instead, several MODTRAN simulations were performed for various optical depths. For these simulations, ~~effective particle~~ particle effective diameter was set to 120 μm, consistently with DARDAR product corresponding to a CALIPSO overpass at 16:10 UTC. The near-surface cloud optical depth was set to 0.07, while the upper cloud optical depth τ was varied from 0.5 to 5 in the calculations. Figure 12c shows that the range $0.5-5$ reproduces quite well the observed variability of brightness temperature. We infer that at small scale cloud variability is extremely high, which is unexpected from satellite data on the large scale for this type of cloud (Grenier et al., 2009). To further investigate the spatial variability, MODIS cloud products ~~(Platnick et al., 2003)~~ at 18:09 UTC were analyzed. In particular, the cloud optical depth and cloud top altitude, shown in Fig. 13, are very instructive. At the scale of Polar 6 spiral, the cloud optical depth is indeed highly variable, ranging from nearly clear sky to values exceeding 5. The cloud top altitude also shows that the probed cloud with top at 5 km was very localized in the most SE section of the spiral~~flight~~. Interestingly, these spatial features are consistent with FIRR observations. In fact, the difference between the temperature measured by the $10-12$ μm channel and the simulation with $\tau = 2$ (indicated by the color of the trajectory in ~~Fig~~Figs. 13a and b) is minimum ~~in~~ near the area corresponding to the high altitude cloud~~. It is higher~~ , which suggests that the cloud there has an optical depth larger than 2. The difference is larger elsewhere, meaning that FIRR senses warmer temperatures corresponding to either a thinner or lower cloud. The variations of the brightness temperature difference are more evident in Fig. 13c, that shows the time series of the difference along with the MODIS estimates of cloud characteristics. Observed FIRR spatial variability is thus consistent with the presence of a cloud of optical depth around 4 in the SE bound of the trajectory that extends up to 5 km. Elsewhere on the trajectory the atmosphere ranges from clear to ~~near-surface~~ low-altitude clouds. The latter also seem to be variable, resulting in slight variations of brightness temperature in the window channels near the surface. This case illustrates the complexity of atmospheric radiative transfer in heterogeneous conditions. It also shows that the FIRR is responding consistently with variations in clouds conditions from a nadir view similar to a satellite view.

4 Discussion

The five case studies investigated in the previous section provided a valuable insight on FIRR performances from an airborne nadir configuration, and on the ~~F-IR~~ FIR characteristics of the Arctic atmosphere in clear and cloudy conditions. To further explore the dependence of FIRR measurements on atmospheric profiles, a series of radiative transfer simulations are performed. The ~~radiative impact of an ice cloud is then investigated in terms of atmospheric cooling rates. The results are~~ results are then discussed in the framework of TICFIRE, with the intent to improve the data quality in future similar airborne campaigns.

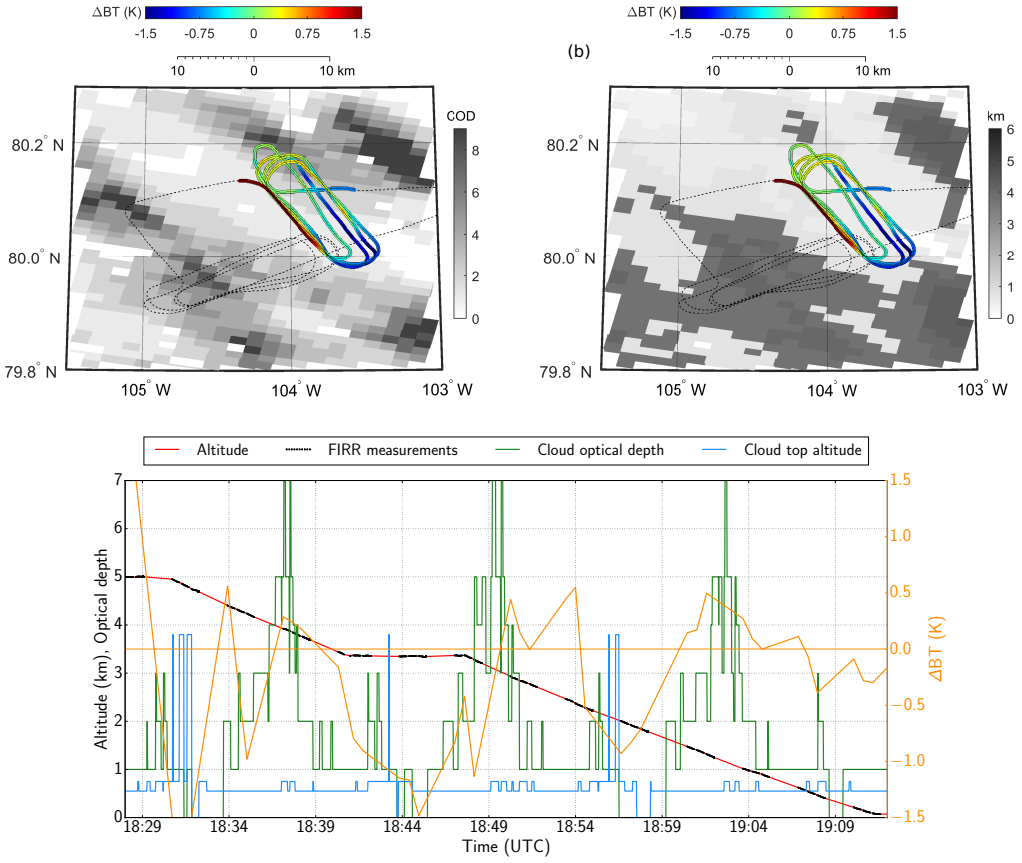

Figure 13. (a) Optical depth at 1.24 μm and (~~b~~bright) cloud top altitude derived from MODIS observations at the beginning of the profile on 13 April (18:09 UTC). Polar 6 trajectory is highlighted, with the color corresponding to the difference between measured and simulated ($\tau = 2$) brightness temperatures for the $10 - 12$ μm channel. Blue ~~means~~ suggests the actual optical depth is ~~less~~ larger than 2 while red ~~means~~ suggests it is ~~larger~~less. (c) Difference between measured and simulated ($\tau = 2$) brightness temperatures for the $10 - 12$ μm channel as a function of time, along with flight altitude and MODIS estimates of cloud optical depth and cloud top altitude. Black dots indicate when FIRR spectral measurements are actually performed.

4.1 Sensitivity to temperature, humidity and cloud properties

In order to extend the interpretation of the data acquired during the NETCARE campaign, the Jacobians of the top of atmosphere (TOA) brightness temperature with respect to temperature and humidity were computed for 11 April simulations (Fig. 14). The Jacobian at a given atmospheric level is the difference in simulated TOA brightness temperature resulting from an increase of 1 K (1% specific humidity) of the temperature (relative humidity) at this level. The temperature Jacobians show that the $30 - 50$ μm channel is mostly sensitive to atmospheric layers below 500 hPa (above $\sim$ 5 km), which explains why this channel was not very useful at lower altitude during the campaign. The shorter ~~F-IR~~ FIR wavelengths are sensitive to lower

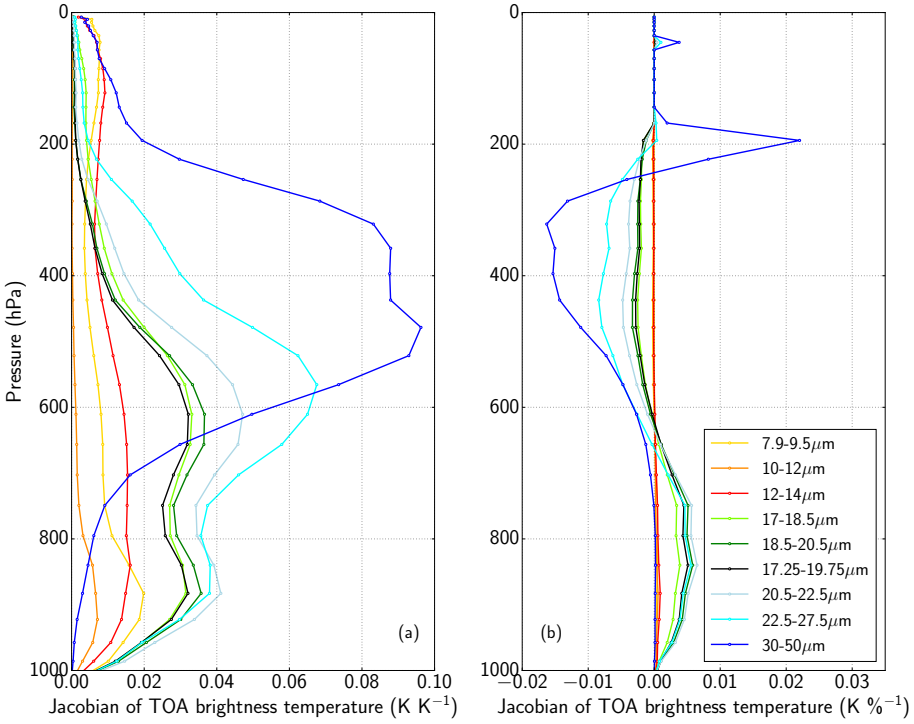

Figure 14. (a) Temperature and (b) humidity Jacobians for the TOA brightness temperature for 11 April atmospheric profile. For humidity, variations are in % of the specific humidity.

layers of the atmosphere, and window channels are almost insensitive to the atmosphere temperature. These Jacobians also suggest that the 3 channels between 17 and 20 μm are very similar, making them ~~somehow~~ somewhat redundant in such atmospheric conditions. Comparing the absolute values of the Jacobians to the FIRR resolution gives a lower estimate of the vertical resolution the FIRR could reach for profiles retrieval applications. ~~Assuming a resolution of~~ Given the radiometric resolution of the FIRR is about 0.2 K, ~~the corresponding vertical resolution approximately varies from~~ temperature variations of 0.2 K are detectable with a vertical resolution of 100 to 200 hPa in ~~F-IR~~ FIR bands. Regarding the FIRR sensitivity to variations in relative humidity, Fig. 14b shows that the $30-50$ μm band is the most sensitive, as expected due to the water vapor absorption spectrum. Humidity variations of 5 % for a 100 hPa thick layer above 600 hPa should produce a detectable signal for all ~~F-IR~~ FIR bands, highlighting the potential of the FIRR for probing humidity profiles in such cold and dry conditions. Note that the Jacobians are positive around the temperature inversion, which is a feature typical of polar conditions. Negative values are consistent with the fact that increasing water vapor increases the greenhouse effect due to the atmosphere and hence decreases radiation at TOA.

To complement this sensitivity analysis, an ice cloud was inserted between 2 and 6 km in the same atmosphere, and the relative humidity with respect to ice correspondingly set to 100 %. Starting from a reference cloud, its optical depth and

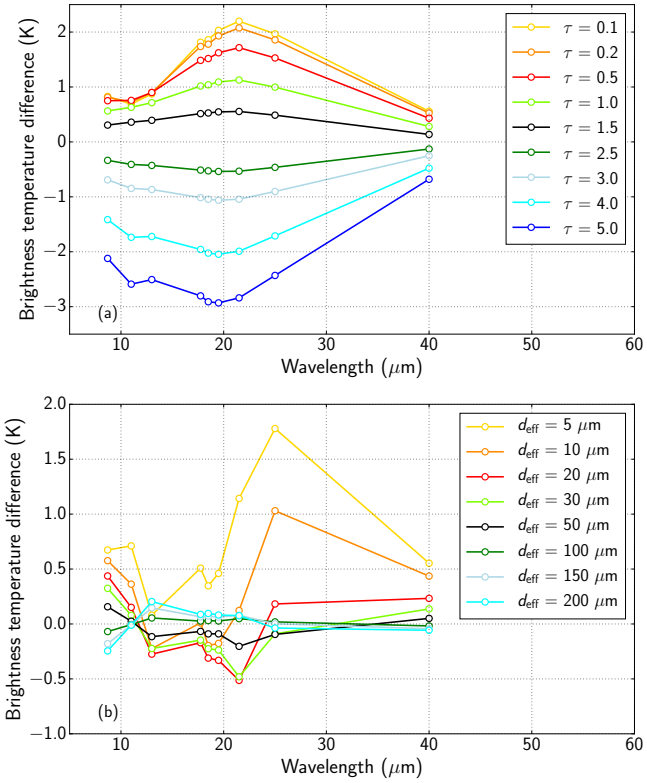

Figure 15. TOA brightness temperature differences between various clouds and the reference with $\tau = 2$ ($\tau = 3$ for panel (b)) and $d_{\text{eff}} = 80$ μm. Panel (a) is for varying optical depth while panel (b) is for varying ~~effective~~ particle effective diameter.

~~effective particle~~ particle effective diameter were varied. Figure 15 shows that TOA ~~F-IR~~ FIR brightness temperatures are very sensitive to cloud optical depth, with variations up to 5 K between clear sky conditions and $\tau = 5$. The FIRR resolution approximately converts into a 0.2 resolution in terms of optical depth. The same exercise with varying optical depth shows that for small particles ~~F-IR~~ FIR channels are very sensitive to particle size. However, the sensitivity quickly decreases for largers sizes, which is consistent with the findings of Yang (2003) and Baran (2007), who suggested a sensitivity up to 100 μm effective dimensions. This sensitivity is directly related to the crystal shape and size distribution assumed for this study, which correspond to cirrus clouds. Although the results above are qualitatively robust, using another ice cloud parameterization could have resulted in different values (e.g. Baran, 2007). In particular, Arctic clouds characterized by rapid crystal growth in high supersaturation conditions may actually have shallower particle size distributions (Jouan et al., 2012) and exhibit more sensitivity to particle size.

4.2 ~~Atmospheric cooling rates~~

Like F-IR radiances, the atmosphere radiative budget is very sensitive to cloud properties. In particular, cloud geometrical and microphysical characteristics largely determine atmospheric cooling rates (Maestri et al., 2005) , in such a complex way that clouds can either warm or cool the atmosphere (Maestri, 2003; Lampert et al., 2009) . Further understanding of the impact of clouds on the atmosphere radiative budget is of primary importance, and direct measurement of the net radiative fluxes is the best approach to this. The net flux was computed from the broadband sensors, and the cooling rates calculated from its vertical variations (e.g. Cox, 1969) . To our knowledge, spectral cooling rates have only been measured once (Mlynczak et al., 2011) . During the NETCARE campaign, the FIRR was supposed to have a zenith view to allow net fluxes computation, but shortly before the campaign started this configuration proved to be incompatible in terms of safety. As a consequence, the spectral cooling rates were simulated for 11 April, with clear sky conditions and with a cloud of optical depth 2 and effective particle diameter 80 μm. Figure **??**a shows that F-IR emission of the atmosphere contributes to cooling the entire atmosphere, resulting in an average 1.5 K day^{-1} cooling in clear sky conditions, which is very consistent with the cooling rates computed from the broadband LW measurements (Fig. **??**b). The presence of an ice cloud enhance this cooling since it acts as an efficient radiator (Fig. **??**c). The corresponding cooling rates are 2-to-3 times larger than in clear sky conditions (Fig. **??**d). Contrary to mid-latitude or tropical conditions, in the absence of solar radiation the cloud radiates more energy than it absorbs from the surface, the latter being too cold to sufficiently warm the cloud. As a consequence, optically thin ice clouds cool the atmosphere in their whole volume, and can dramatically affect the stability of the atmosphere (Blanchet et al., 2011) .

Simulated spectral cooling rates for 11 April atmosphere for (a) clear sky and (c) cloudy ($\tau = 2$) conditions. The dark horizontal lines in panel (c) and (d) indicate cloud bottom and top heights. Units is $100 \times$ K day^{-1} μm^{-1}. Simulated broadband cooling rates are also shown (b and d). Broadband cooling rates computed from broadband LW measurements are shown in panel (b).

4.2 Recommendations for future operation

The preceding results are now discussed in the framework of planning the TICFIRE satellite mission and in view of future airborne campaigns with the FIRR or similar instruments. First of all, one advantage of using uncooled microbolometers is the possibility to have an imager, as will be the case for TICFIRE. In this study, the FIRR was not used as an imager, though, because it has a much narrower field of ~~fiew~~ view than TICFIRE satellite configuration. However it is worth exploring how the accuracy of the measurements would decay if spatial averaging was skipped. To this end, the spectral brightness temperature shown in Fig. 7 is computed again from FIRR measurements, except that spatial averaging is made on 1 (no averaging), 4, 9 or 193 pixels. Nominal data processing is optimized for 193 pixels and could not be applied to a single pixel (Libois et al., 2016), so that the procedure was slightly changed to ensure that the same calibration is applied independently of the number of pixels averaged. The results are shown in Fig. 16. As expected, spatial averaging improves the repeatability of the measurement, but averaging over 9 pixels already provides a resolution close to 193 pixels. The absolute values are very consistent, with differences less than 0.5 K if more than 1 pixel are used. The remaining differences can be attributed to instrument errors, but scene spatial heterogeneities can not be ruled out. This suggests that the present study is relevant to verify the performances of the future TICFIRE satellite instrument, whose precision could be increased through spatial averaging over neighbour pixels.

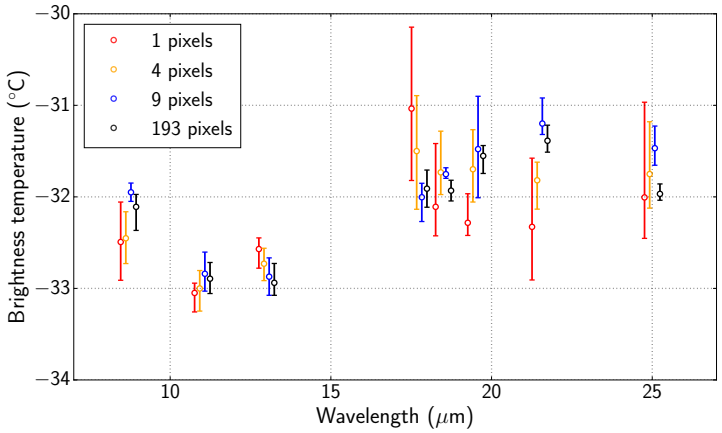

Figure 16. FIRR spectral brightness temperatures at 5.56 km as in Fig. 7, except that measurements were averaged over a varying number of pixels, from 1 to 193. Error bars indicate measurement variability along 4 consecutive measurements. For each spectral band the 4 corresponding error bars are slightly displaced horizontally for sake of clarity.

It is worth pointing out that the NETCARE campaign was not dedicated solely to radiation measurements. Probing ice clouds was one of the objectives, but not the only one. In addition, few clouds were encountered during the campaign and days with too many clouds prevented aircraft operations for safety reasons. Overall the dataset is still modest and further campaigns in the Arctic winter remain necessary, in particular to complete a radiative closure in cloudy conditions, which was not possible here due to lack of quantitative information about clouds properties. Such campaigns should be dedicated to the radiative properties of ice clouds in order to maximize the scientific success of this research topic (e.g. CIRCCREX, Fox, 2015). During the NETCARE campaign, the FIRR was supposed to have a zenith view to allow net fluxes computation and associated cooling rates, but shortly before the campaign started this configuration proved to be incompatible in terms of safety. In the future, combining nadir and zenith views as in Mlynczak et al. (2011) would be extremely beneficial to the understanding of the atmospheric radiative budget in the FIR. From the FIRR perspective, we noticed that upgrading the current instrument radiometric resolution is essential to further constrain radiative transfer simulations and cloud properties retrievals. This can be achieved by improving the environmental conditions of the FIRR within the aircraft, paying more attention to temperature stability. Adding an insulating window to prevent air circulation around the instrument or increasing the pressure inside the instrument to ensure constant outflow from the aircraft would minimize temperature variations. Note that these recommendations are linked to the fact that Polar 6 cabin is unpressurized and other constraints should be thought of in the case of a pressurized aircraft. Complementary zenith and nadir observations would also be extremely valuable in order to compute cooling rates and sample the whole atmospheric profile.

At the instrument level, the FIRR is the first prototype and improvements are expected from technological developments of uncooled microbolometers, but optimization in the analogical-numerical converter and absence of the detector window in space could already increase the current resolution by a factor of 3 to 5. Likewise, increasing acquisition rate by using a faster

filter wheel and scene selection motor would reduce the acquisition time of a sequence by one order of magnitude, thus limiting temperature variations in between calibrations. ~~Such~~ It would also ensure that measurements in all channels are taken on the same target, which was not always the case during the campaign above leads or through highly heterogeneous ice clouds. Such technical developments are already considered and will be mandatory for the satellite version of the instrument which requires acquisition times around 1 s for a complete scene sequence.

5 Conclusions

The first airborne campaign of the FIRR took place in the Arctic ~~and~~ in the framework of the NETCARE aircraft campaign. It was a great opportunity to study the ~~far-infrared~~ radiative properties of the early spring Arctic atmosphere, and highlighted the importance of water vapor and ice clouds in this remote environment. Vertical profiles of brightness temperature acquired in clear sky and cloudy conditions provided a strong observational constraint on the radiative properties. At the same time, they increased the limited amount of observations available in the far-infrared, especially in such remote regions. These observations also provided valuable knowledge about the FIRR instrument, which can be used to improve operation and development in view of the TICFIRE satellite mission. This campaign showed that the current state-of-the-art radiative transfer models are well suited for the Arctic and confirm that instrument resolution is better than the uncertainties inherent to the radiative transfer formulation and input observations. They also show that aerosols can significantly impact the radiative budget of the atmosphere, thus implying that a detailed characterization of the aerosols and haze is necessary to refine radiative closure experiments. Although the FIRR behaved very well during the campaign with respect to its nominal performances, the latter could be improved for accurate retrievals of atmospheric and cloud characteristics. The campaign proved that ice clouds in the Arctic are hard to probe, as much for reasons of safety as for their complexity and their high heterogeneity. ~~Such~~ As a consequence, measured ice clouds spectral signature could not be compared to simulations with sufficiently well-constrained cloud properties. Such airborne campaigns should be replicated to improve our understanding of ice cloud formation and radiative properties in polar regions. Accordingly, they should be dedicated to radiation and combine cloud microphysical observations with various radiation sensors. Such studies are necessary to continue improving our knowledge of ice cloud formation and its parameterization in numerical weather prediction and climate models.

Data availability

All NETCARE data will be made public after the end of the project (http://www.netcare-project.ca). In the meantime, access can be granted by contacting the project manager Bob Christensen (bob.christensen@utoronto.ca). The FIRR data used in this study are available upon request from the authors (libois.quentin@uqam.ca). Requests for access to AWI data should be sent to Martin Gehrmann (martin.gehrmann@awi.de). The CALIPSO and DARDAR products were obtained from the ICARE Data Center (http://www.icare.univ-lille1.fr/). MODIS data were obtained from LAADS (https://ladsweb.nascom.nasa.gov/).

Author contributions. Q. Libois, L. Ivanescu and H. Schulz operated the FIRR during the airborne campaign. H. Bozem and W. R. Leaitch were scientific leaders aboard Polar 6 and responsible for gas measurements and cloud probes, respectively. J. Burkart and A. A. Aliabadi processed the meteorological and aircraft data. Q. Libois and L. Ivanescu processed the data and Q. Libois performed the radiative transfer simulations. Q. Libois wrote the manuscript with contributions of all co-authors.

Acknowledgements. This research was funded jointly by the Canadian Space Agency (CSA) through the FAST program, by NETCARE through the Climate Change and Atmospheric Research (CCAR) program at the Natural Sciences and Engineering Research Council of Canada (NSERC), by the Alfred Wegener Institute (AWI) and by Environment and Climate Change Canada (ECCC). We are grateful to the editor for his support and acknowledge the two reviewers who helped improve the quality of the manuscript. We thank the Nunavut Research Institute and the Nunavut Impact Review Board for licensing the study. We thank Kenn Borek Air Ltd (KBAL), in particular Gary Murtsell and Neil Travers for their skillful piloting across the Arctic. We acknowledge Martin Gehrmann, Manuel Sellmann and Lukas Kandora (AWI) for their technical help during airborne operation. We thank Alexei Korolev (ECCC) for providing Nevzorov and 2D-C probes data and Gerit Birnbaum (AWI) for helping with the processing of AWI radiation sensors. Norm O'Neill (Université de Sherbrooke) accommodated the involvement of L. Ivanescu to the campaign. Canadian Network for the Detection of Atmospheric Change (CANDAC), to which L. Ivanescu is affiliated, provided logistic support during the stay at Eureka Weather Station. The Institut National d'Optique (INO) provided technical support for the FIRR before and during the campaign. We are grateful to Marcus Dejmek and Daniel Gratton (CSA) for providing logistic resources for the FIRR. We are indebted to Mike Harwood (ECCC) for his direction of the instrument integration and support in the field. We also thank John Ford, David Heath and the University of Toronto machine shop, Jim Hodgson and Lake Central Air Services (LCAS) in Muskoka, Jim Watson (Scale Modelbuilders, Inc.), Andrew Elford (ECCC) and Julia Binder (AWI) for their support of the instrument integration. We are grateful to Bob Christensen (U. Toronto), Doug MacKenzie (KBAL), Rosa Wu, Carrie Taylor, Sangeeta Sharma, Desiree Toom, Dan Veber, Alina Chivulescu, Andrew Platt, Ralf Staebler, Anne Marie Macdonald and Maurice Watt (ECCC) for their support of the study. We acknowledge modelling support from MPIC and University of Mainz, Mainz (Daniel Kunkel, Jens Krause and Franziska Köllner) and U. of Quebec at Montreal (Ana Cirisan and a class of students) used for flight planning. We thank the Biogeochemistry department of MPIC for providing the CO instrument and Dieter Scharffe for his support during the preparation phase of the campaign.

References

Aliabadi, A. A., Staebler, R. M., Liu, M., and Herber, A.: Characterization and Parametrization of Reynolds Stress and Turbulent Heat Flux in the Stably-Stratified Lower Arctic Troposphere Using Aircraft Measurements, Boundary-Layer Meteorology, doi:10.1007/s10546-016-0164-7, http://link.springer.com/10.1007/s10546-016-0164-7, 2016.

Aumann, H., Chahine, M., Gautier, C., Goldberg, M., Kalnay, E., McMillin, L., Revercomb, H., Rosenkranz, P., Smith, W., Staelin, D., Strow, L., and Susskind, J.: AIRS/AMSU/HSB on the aqua mission: design, science objectives, data products, and processing systems, IEEE Transactions on Geoscience and Remote Sensing, 41, 253–264, doi:10.1109/TGRS.2002.808356, http://ieeexplore.ieee.org/lpdocs/epic03/wrapper.htm?arnumber=1196043, 2003.

Baran, A. J.: The impact of cirrus microphysical and macrophysical properties on upwelling far-infrared spectra, Quarterly Journal of the Royal Meteorological Society, 133, 1425–1437, doi:10.1002/qj.132, http://doi.wiley.com/10.1002/qj.132, 2007.

Berk, A., Anderson, G. P., Acharya, P. K., Bernstein, L. S., Muratov, L., Lee, J., Fox, M., Adler-Golden, S. M., Chetwynd, J. H., Hoke, M. L., Lockwood, R. B., Gardner, J. A., Cooley, T. W., Borel, C. C., and Lewis, P. E.: MODTRAN 5: a reformulated atmospheric band model with auxiliary species and practical multiple scattering options: update, p. 662, doi:10.1117/12.606026, http://proceedings.spiedigitallibrary.org/proceeding.aspx?doi=10.1117/12.606026, 2005.

Bianchini, G., Palchetti, L., Muscari, G., Fiorucci, I., Di Girolamo, P., and Di Iorio, T.: Water vapor sounding with the far infrared REFIR-PAD spectroradiometer from a high-altitude ground-based station during the ECOWAR campaign, Journal of Geophysical Research, 116, doi:10.1029/2010JD014530, http://doi.wiley.com/10.1029/2010JD014530, 2011.

Blanchard, Y., Royer, A., O'neill, N. T., and Blanchet, J.-P.: Retrieving cloud optical depth and ice particle size using thermal and Far infrered radiometry in an Arctic environment, pp. III–849–III–852, IEEE, doi:10.1109/IGARSS.2009.5417902, http://ieeexplore.ieee.org/lpdocs/epic03/wrapper.htm?arnumber=5417902, 2009.

Blanchet, J.-P., Royer, A., Châteauneuf, F., Bouzid, Y., Blanchard, Y., Hamel, J.-F., de Lafontaine, J., Gauthier, P., O'Neill, N. T., Pancrati, O., and Garand, L.: TICFIRE: a far infrared payload to monitor the evolution of thin ice clouds, pp. 81 761K–81 761K–11, doi:10.1117/12.898577, http://proceedings.spiedigitallibrary.org/proceeding.aspx?articleid=1343190, 2011.

Blumstein, D., Chalon, G., Carlier, T., Buil, C., Hebert, P., Maciaszek, T., Ponce, G., Phulpin, T., Tournier, B., Simeoni, D., Astruc, P., Clauss, A., Kayal, G., and Jegou, R.: IASI instrument: technical overview and measured performances, pp. 196–207, doi:10.1117/12.560907, http://proceedings.spiedigitallibrary.org/proceeding.aspx?articleid=1318774, 2004.

Canas, T. A., Murray, J. E., and Harries, J. E.: Tropospheric airborne Fourier transform spectrometer (TAFTS), pp. 91–102, doi:10.1117/12.301139, http://proceedings.spiedigitallibrary.org/proceeding.aspx?articleid=932527, 1997.

Chen, X., Huang, X., and Flanner, M. G.: Sensitivity of modeled far-IR radiation budgets in polar continents to treatments of snow surface and ice cloud radiative properties, Geophysical Research Letters, 41, 6530–6537, doi:10.1002/2014GL061216, http://doi.wiley.com/10.1002/2014GL061216, 2014.

Clough, S., Shephard, M., Mlawer, E., Delamere, J., Iacono, M., Cady-Pereira, K., Boukabara, S., and Brown, P.: Atmospheric radiative transfer modeling: a summary of the AER codes, Journal of Quantitative Spectroscopy and Radiative Transfer, 91, 233–244, doi:10.1016/j.jqsrt.2004.05.058, http://linkinghub.elsevier.com/retrieve/pii/S0022407304002158, 2005.

Clough, S. A., Iacono, M. J., and Moncet, J.-L.: Line-by-line calculations of atmospheric fluxes and cooling rates: Application to water vapor, Journal of Geophysical Research, 97, 15 761, doi:10.1029/92JD01419, http://doi.wiley.com/10.1029/92JD01419, 1992.

Conrath, B. J., Hanel, R. A., Kunde, V. G., and Prabhakara, C.: The Infrared Interferometer Experiment on Nimbus 3, Journal of Geophysical Research, 75, 5831–5857, doi:10.1029/JC075i030p05831, http://doi.wiley.com/10.1029/JC075i030p05831, 1970.

Cox, C. J., Turner, D. D., Rowe, P. M., Shupe, M. D., and Walden, V. P.: Cloud Microphysical Properties Retrieved from Downwelling Infrared Radiance Measurements Made at Eureka, Nunavut, Canada (2006–09), Journal of Applied Meteorology and Climatology, 53, 772–791, doi:10.1175/JAMC-D-13-0113.1, http://journals.ametsoc.org/doi/abs/10.1175/JAMC-D-13-0113.1, 2014.

Cox, C. J., Walden, V. P., Rowe, P. M., and Shupe, M. D.: Humidity trends imply increased sensitivity to clouds in a warming Arctic, Nature Communications, 6, 10 117, doi:10.1038/ncomms10117, http://www.nature.com/doifinder/10.1038/ncomms10117, 2015.

Cox, C. V., Harries, J. E., Taylor, J. P., Green, P. D., Baran, A. J., Pickering, J. C., Last, A. E., and Murray, J.: Measurement and simulation of mid- and far-infrared spectra in the presence of cirrus, Quarterly Journal of the Royal Meteorological Society, pp. n/a–n/a, doi:10.1002/qj.596, http://doi.wiley.com/10.1002/qj.596, 2010.

Cox, S. K.: Observational Evidence of Anomalous Infrared Cooling in a Clear Tropical Atmosphere, Journal of the Atmospheric Sciences, 26, 1347–1349, doi:10.1175/1520-0469(1969)026<1347:OEOAIC>2.0.CO;2, http://journals.ametsoc.org/doi/abs/10.1175/1520-0469%281969%29026%3C1347%3AOEOAIC%3E2.0.CO%3B2, 1969.

Dee, D. P., Uppala, S. M., Simmons, A. J., Berrisford, P., Poli, P., Kobayashi, S., Andrae, U., Balmaseda, M. A., Balsamo, G., Bauer, P., Bechtold, P., Beljaars, A. C. M., van de Berg, L., Bidlot, J., Bormann, N., Delsol, C., Dragani, R., Fuentes, M., Geer, A. J., Haimberger, L., Healy, S. B., Hersbach, H., Hólm, E. V., Isaksen, L., Kållberg, P., Köhler, M., Matricardi, M., McNally, A. P., Monge-Sanz, B. M., Morcrette, J.-J., Park, B.-K., Peubey, C., de Rosnay, P., Tavolato, C., Thépaut, J.-N., and Vitart, F.: The ERA-Interim reanalysis: configuration and performance of the data assimilation system, Quarterly Journal of the Royal Meteorological Society, 137, 553–597, doi:10.1002/qj.828, http://doi.wiley.com/10.1002/qj.828, 2011.

Delamere, J. S., Clough, S. A., Payne, V. H., Mlawer, E. J., Turner, D. D., and Gamache, R. R.: A far-infrared radiative closure study in the Arctic: Application to water vapor, Journal of Geophysical Research, 115, doi:10.1029/2009JD012968, http://doi.wiley.com/10.1029/2009JD012968, 2010.

Delanoë, J. and Hogan, R. J.: Combined CloudSat-CALIPSO-MODIS retrievals of the properties of ice clouds, Journal of Geophysical Research, 115, doi:10.1029/2009JD012346, http://doi.wiley.com/10.1029/2009JD012346, 2010.

Ehrlich, A. and Wendisch, M.: Reconstruction of high-resolution time series from slow-response broadband terrestrial irradiance measurements by deconvolution, Atmospheric Measurement Techniques, 8, 3671–3684, doi:10.5194/amt-8-3671-2015, http://www.atmos-meas-tech.net/8/3671/2015/, 2015.

Emery, W. J., Good, W. S., Tandy, W., Izaguirre, M. A., and Minnett, P. J.: A Microbolometer Airborne Calibrated Infrared Radiometer: The Ball Experimental Sea Surface Temperature (BESST) Radiometer, IEEE Transactions on Geoscience and Remote Sensing, 52, 7775–7781, doi:10.1109/TGRS.2014.2318683, http://ieeexplore.ieee.org/lpdocs/epic03/wrapper.htm?arnumber=6822518, 2014.

Feldman, D. R., Collins, W. D., Pincus, R., Huang, X., and Chen, X.: Far-infrared surface emissivity and climate, Proceedings of the National Academy of Sciences, 111, 16 297–16 302, doi:10.1073/pnas.1413640111, http://www.pnas.org/lookup/doi/10.1073/pnas.1413640111, 2014.

Fox, C.: Far-infrared spectral radiance studies: Application to water vapour and cirrus, Ph.D. thesis, 2015.

Fox, C., Green, P. D., Pickering, J. C., and Humpage, N.: Analysis of far-infrared spectral radiance observations of the water vapor continuum in the Arctic, Journal of Quantitative Spectroscopy and Radiative Transfer, 155, 57–65, doi:10.1016/j.jqsrt.2015.01.001, http://linkinghub.elsevier.com/retrieve/pii/S0022407315000023, 2015.

Garand, L., Turner, D. S., Larocque, M., Bates, J., Boukabara, S., Brunel, P., Chevallier, F., Deblonde, G., Engelen, R., Hollingshead, M., Jackson, D., Jedlovec, G., Joiner, J., Kleespies, T., McKague, D. S., McMillin, L., Moncet, J.-L., Pardo, J. R., Rayer, P. J., Salathe, E., Saunders, R., Scott, N. A., Van Delst, P., and Woolf, H.: Radiance and Jacobian intercomparison of radiative transfer models applied to HIRS and AMSU channels, Journal of Geophysical Research: Atmospheres, 106, 24 017–24 031, doi:10.1029/2000JD000184, http://doi.wiley.com/10.1029/2000JD000184, 2001.

Green, P. D., Newman, S. M., Beeby, R. J., Murray, J. E., Pickering, J. C., and Harries, J. E.: Recent advances in measurement of the water vapour continuum in the far-infrared spectral region, Philosophical Transactions of the Royal Society A: Mathematical, Physical and Engineering Sciences, 370, 2637–2655, doi:10.1098/rsta.2011.0263, http://rsta.royalsocietypublishing.org/cgi/doi/10.1098/rsta.2011.0263, 2012.

Grenier, P., Blanchet, J., and Munoz-Alpizar, R.: Study of polar thin ice clouds and aerosols seen by CloudSat and CALIPSO during mid-winter 2007, Journal of Geophysical Research, 114, doi:10.1029/2008JD010927, http://doi.wiley.com/10.1029/2008JD010927, 2009.

Harries, J., Carli, B., Rizzi, R., Serio, C., Mlynczak, M., Palchetti, L., Maestri, T., Brindley, H., and Masiello, G.: The Far-infrared Earth, Reviews of Geophysics, 46, doi:10.1029/2007RG000233, http://doi.wiley.com/10.1029/2007RG000233, 2008.

Huang, Y., Leroy, S., Gero, P. J., Dykema, J., and Anderson, J.: Separation of longwave climate feedbacks from spectral observations, Journal of Geophysical Research, 115, doi:10.1029/2009JD012766, http://doi.wiley.com/10.1029/2009JD012766, 2010.

Jouan, C., Girard, E., Pelon, J., Gultepe, I., Delanoë, J., and Blanchet, J.-P.: Characterization of Arctic ice cloud properties observed during ISDAC, Journal of Geophysical Research, 117, doi:10.1029/2012JD017889, http://doi.wiley.com/10.1029/2012JD017889, 2012.

King, M., Menzel, W., Kaufman, Y., Tanre, D., Bo-Cai Gao, Platnick, S., Ackerman, S., Remer, L., Pincus, R., and Hubanks, P.: Cloud and aerosol properties, precipitable water, and profiles of temperature and water vapor from MODIS, IEEE Transactions on Geoscience and Remote Sensing, 41, 442–458, doi:10.1109/TGRS.2002.808226, http://ieeexplore.ieee.org/lpdocs/epic03/wrapper.htm?arnumber=1196060, 2003.

Knuteson, R. O., Revercomb, H. E., Best, F. A., Ciganovich, N. C., Dedecker, R. G., Dirkx, T. P., Ellington, S. C., Feltz, W. F., Garcia, R. K., Howell, H. B., Smith, W. L., Short, J. F., and Tobin, D. C.: Atmospheric Emitted Radiance Interferometer. Part I: Instrument Design, Journal of Atmospheric and Oceanic Technology, 21, 1763–1776, doi:10.1175/JTECH-1662.1, http://journals.ametsoc.org/doi/abs/10.1175/JTECH-1662.1, 2004.

Korolev, A. V., Strapp, J. W., Isaac, G. A., and Nevzorov, A. N.: The Nevzorov Airborne Hot-Wire LWC–TWC Probe: Principle of Operation and Performance Characteristics, Journal of Atmospheric and Oceanic Technology, 15, 1495–1510, doi:10.1175/1520-0426(1998)015<1495:TNAHWL>2.0.CO;2, http://journals.ametsoc.org/doi/abs/10.1175/1520-0426%281998%29015%3C1495%3ATNAHWL%3E2.0.CO%3B2, 1998.

Lampert, A., Ehrlich, A., Dörnbrack, A., Jourdan, O., Gayet, J.-F., Mioche, G., Shcherbakov, V., Ritter, C., and Wendisch, M.: Microphysical and radiative characterization of a subvisible midlevel Arctic ice cloud by airborne observations – a case study, Atmospheric Chemistry and Physics, 9, 2647–2661, doi:10.5194/acp-9-2647-2009, http://www.atmos-chem-phys.net/9/2647/2009/, 2009.

Leaitch, W. R., Korolev, A., Aliabadi, A. A., Burkart, J., Willis, M., Abbatt, J. P. D., Bozem, H., Hoor, P., Köllner, F., Schneider, J., Herber, A., Konrad, C., and Brauner, R.: Effects of 20-100 nanometre particles on liquid clouds in the clean summertime Arctic, Atmospheric Chemistry and Physics Discussions, pp. 1–50, doi:10.5194/acp-2015-999, http://www.atmos-chem-phys-discuss.net/acp-2015-999/, 2016.

Libois, Q., Proulx, C., Ivanescu, L., Coursol, L., Pelletier, L. S., Bouzid, Y., Barbero, F., Girard, E., and Blanchet, J.-P.: A microbolometer-based far infrared radiometer to study thin ice clouds in the Arctic, Atmospheric Measurement Techniques, 9, 1817–1832, doi:10.5194/amt-9-1817-2016, http://www.atmos-meas-tech.net/9/1817/2016/, 2016.

Liuzzi, G., Masiello, G., Serio, C., Palchetti, L., and Bianchini, G.: Validation of H2O Continuum Absorption Models in the Wave Number Range 180–600 cm-1 with Atmospheric Emitted Spectral Radiance Measured at the Antarctica Dome-C Site, Optics Express, 22, 16 784, doi:10.1364/OE.22.016784, https://www.osapublishing.org/oe/abstract.cfm?uri=oe-22-14-16784, 2014.

Maestri, T.: A study of infrared diabatic forcing of ice clouds in the tropical atmosphere, Journal of Geophysical Research, 108, doi:10.1029/2002JD002146, http://doi.wiley.com/10.1029/2002JD002146, 2003.

Maestri, T., Rizzi, R., and Smith, J. A.: Spectral infrared analysis of a cirrus cloud based on Airborne Research Interferometer Evaluation System (ARIES) measurements: SPECTRAL INFRARED ANALYSIS OF A CIRRUS CLOUD, Journal of Geophysical Research: Atmospheres, 110, n/a–n/a, doi:10.1029/2004JD005098, http://doi.wiley.com/10.1029/2004JD005098, 2005.

Maestri, T., Rizzi, R., Tosi, E., Veglio, P., Palchetti, L., Bianchini, G., Di Girolamo, P., Masiello, G., Serio, C., and Summa, D.: Analysis of cirrus cloud spectral signatures in the far infrared, Journal of Quantitative Spectroscopy and Radiative Transfer, 141, 49–64, doi:10.1016/j.jqsrt.2014.02.030, http://linkinghub.elsevier.com/retrieve/pii/S0022407314000879, 2014.

Mariani, Z., Strong, K., Wolff, M., Rowe, P., Walden, V., Fogal, P. F., Duck, T., Lesins, G., Turner, D. S., Cox, C., Eloranta, E., Drummond, J. R., Roy, C., Turner, D. D., Hudak, D., and Lindenmaier, I. A.: Infrared measurements in the Arctic using two Atmospheric Emitted Radiance Interferometers, Atmospheric Measurement Techniques, 5, 329–344, doi:10.5194/amt-5-329-2012, http://www.atmos-meas-tech.net/5/329/2012/, 2012.

Marty, C.: Downward longwave irradiance uncertainty under arctic atmospheres: Measurements and modeling, Journal of Geophysical Research, 108, doi:10.1029/2002JD002937, http://doi.wiley.com/10.1029/2002JD002937, 2003.

McCleese, D. J., Schofield, J. T., Taylor, F. W., Calcutt, S. B., Foote, M. C., Kass, D. M., Leovy, C. B., Paige, D. A., Read, P. L., and Zurek, R. W.: Mars Climate Sounder: An investigation of thermal and water vapor structure, dust and condensate distributions in the atmosphere, and energy balance of the polar regions, Journal of Geophysical Research, 112, doi:10.1029/2006JE002790, http://doi.wiley.com/10.1029/2006JE002790, 2007.

Merrelli, A. and Turner, D. D.: Comparing Information Content of Upwelling Far-Infrared and Midinfrared Radiance Spectra for Clear Atmosphere Profiling, Journal of Atmospheric and Oceanic Technology, 29, 510–526, doi:10.1175/JTECH-D-11-00113.1, http://journals.ametsoc.org/doi/abs/10.1175/JTECH-D-11-00113.1, 2012.

Mlawer, E. J., Payne, V. H., Moncet, J.-L., Delamere, J. S., Alvarado, M. J., and Tobin, D. C.: Development and recent evaluation of the MT_CKD model of continuum absorption, Philosophical Transactions of the Royal Society A: Mathematical, Physical and Engineering Sciences, 370, 2520–2556, doi:10.1098/rsta.2011.0295, http://rsta.royalsocietypublishing.org/cgi/doi/10.1098/rsta.2011.0295, 2012.

Mlynczak, M., Johnson, D. G., and Cageao, R. P.: Scientific Results from the FIRST Instrument Deployment to Cerro Toco, Chile and from the Flight of the INFLAME Instrument, p. HMB1, OSA, doi:10.1364/HISE.2011.HMB1, https://www.osapublishing.org/abstract.cfm?uri=HISE-2011-HMB1, 2011.

Mlynczak, M. G., Harries, J. E., Rizzi, R., Stackhouse, P. W., Kratz, D. P., Johnson, D. G., Mertens, C. J., Garcia, R. R., and Soden, B. J.: Far-infrared: a frontier in remote sensing of Earth's climate and energy balance, pp. 150–158, doi:10.1117/12.454247, http://proceedings.spiedigitallibrary.org/proceeding.aspx?articleid=893229, 2002.

Mlynczak, M. G., Johnson, D. G., Latvakoski, H., Jucks, K., Watson, M., Kratz, D. P., Bingham, G., Traub, W. A., Wellard, S. J., Hyde, C. R., and Liu, X.: First light from the Far-Infrared Spectroscopy of the Troposphere (FIRST) instrument, Geophysical Research Letters, 33, doi:10.1029/2005GL025114, http://doi.wiley.com/10.1029/2005GL025114, 2006.

Mlynczak, M. G., Cageao, R. P., Mast, J. C., Kratz, D. P., Latvakoski, H., and Johnson, D. G.: Observations of downwelling far-infrared emission at Table Mountain California made by the FIRST instrument, Journal of Quantitative Spectroscopy and Radiative Transfer, 170, 90–105, doi:10.1016/j.jqsrt.2015.10.017, http://linkinghub.elsevier.com/retrieve/pii/S0022407315300340, 2016.

Ngo Phong, L., Proulx, C., Oulachgar, H., and Châteauneuf, F.: Far infrared microbolometers for radiometric measurements of ice cloud, p. 93750G, doi:10.1117/12.2076219, http://proceedings.spiedigitallibrary.org/proceeding.aspx?doi=10.1117/12.2076219, 2015.

O'Neill, N. T., Eck, T. F., Smirnov, A., Holben, B. N., and Thulasiraman, S.: Spectral discrimination of coarse and fine mode optical depth, Journal of Geophysical Research: Atmospheres, 108, 2003.

Paige, D. A., Foote, M. C., Greenhagen, B. T., Schofield, J. T., Calcutt, S., Vasavada, A. R., Preston, D. J., Taylor, F. W., Allen, C. C., Snook, K. J., Jakosky, B. M., Murray, B. C., Soderblom, L. A., Jau, B., Loring, S., Bulharowski, J., Bowles, N. E., Thomas, I. R., Sullivan, M. T., Avis, C., De Jong, E. M., Hartford, W., and McCleese, D. J.: The Lunar Reconnaissance Orbiter Diviner Lunar Radiometer Experiment, Space Science Reviews, 150, 125–160, doi:10.1007/s11214-009-9529-2, http://link.springer.com/10.1007/s11214-009-9529-2, 2010.

Palchetti, L., Barbis, A., Harries, J., and Lastrucci, D.: Design and mathematical modelling of the space-borne far-infrared Fourier transform spectrometer for REFIR experiment, Infrared Physics & Technology, 40, 367–377, doi:10.1016/S1350-4495(99)00026-2, http://linkinghub.elsevier.com/retrieve/pii/S1350449599000262, 1999.

Palchetti, L., Belotti, C., Bianchini, G., Castagnoli, F., Carli, B., Cortesi, U., Pellegrini, M., Camy-Peyret, C., Jeseck, P., and Té, Y.: Technical note: First spectral measurement of the Earth's upwelling emission using an uncooled wideband Fourier transform spectrometer, Atmospheric Chemistry and Physics, 6, 5025–5030, doi:10.5194/acp-6-5025-2006, http://www.atmos-chem-phys.net/6/5025/2006/, 2006.

Palchetti, L., Bianchini, G., Di Natale, G., and Del Guasta, M.: Far infrared radiative properties of water vapor and clouds in Antarctica, Bulletin of the American Meteorological Society, p. 150327084825001, doi:10.1175/BAMS-D-13-00286.1, http://journals.ametsoc.org/doi/abs/10.1175/BAMS-D-13-00286.1, 2015.

Palchetti, L., Di Natale, G., and Bianchini, G.: Remote sensing of cirrus cloud microphysical properties using spectral measurements over the full range of their thermal emission: CIRRUS CLOUD FAR IR SIGNATURE, 121, 10,804–10,819, doi:10.1002/2016JD025162, http://doi.wiley.com/10.1002/2016JD025162, 2016.

Platnick, S., King, M., Ackerman, S., Menzel, W., Baum, B., Riedi, J., and Frey, R.: The MODIS cloud products: algorithms and examples from terra, IEEE Transactions on Geoscience and Remote Sensing, 41, 459–473, doi:10.1109/TGRS.2002.808301, http://ieeexplore.ieee.org/lpdocs/epic03/wrapper.htm?arnumber=1196061, 2003.

Rathke, C.: Improving IR cloud phase determination with 20 microns spectral observations, Geophysical Research Letters, 29, doi:10.1029/2001GL014594, http://doi.wiley.com/10.1029/2001GL014594, 2002.

Ritter, C., Notholt, J., Fischer, J., and Rathke, C.: Direct thermal radiative forcing of tropospheric aerosol in the Arctic measured by ground based infrared spectrometry, Geophysical Research Letters, 32, doi:10.1029/2005GL024331, http://doi.wiley.com/10.1029/2005GL024331, 2005.

Rizzi, R., Serio, C., and Amorati, R.: Sensitivity of broadband and spectral measurements of outgoing radiance to changes in water vapor content, pp. 181–190, doi:10.1117/12.454250, http://proceedings.spiedigitallibrary.org/proceeding.aspx?articleid=893237, 2002.

Sauvage, L., Flamant, P. H., Chepfer, H., Brogniez, G., Trouillet, V., Pelon, J., and Albers, F.: Remote Sensing of Cirrus Radiative Parameters during EUCREX'94. Case Study of 17 April 1994. Part I: Observations, Monthly Weather Review, 127, 486–503, doi:10.1175/1520-0493(1999)127<0486:RSOCRP>2.0.CO;2, http://journals.ametsoc.org/doi/abs/10.1175/1520-0493%281999%29127%3C0486%3ARSOCRP%3E2.0.CO%3B2, 1999.

Schwarz, J. P., Gao, R. S., Fahey, D. W., Thomson, D. S., Watts, L. A., Wilson, J. C., Reeves, J. M., Darbeheshti, M., Baumgardner, D. G., Kok, G. L., Chung, S. H., Schulz, M., Hendricks, J., Lauer, A., Kärcher, B., Slowik, J. G., Rosenlof, K. H., Thompson, T. L., Langford, A. O., Loewenstein, M., and Aikin, K. C.: Single-particle measurements of midlatitude black carbon and light-scattering aerosols from the boundary layer to the lower stratosphere, Journal of Geophysical Research, 111, doi:10.1029/2006JD007076, http://doi.wiley.com/10.1029/2006JD007076, 2006.

Shahabadi, M. B. and Huang, Y.: Measuring Stratospheric H_2O with an Airborne Spectrometer, Journal of Atmospheric and Oceanic Technology, 31, 1502–1515, doi:10.1175/JTECH-D-13-00191.1, http://journals.ametsoc.org/doi/abs/10.1175/JTECH-D-13-00191.1, 2014.

Shine, K. P., Ptashnik, I. V., and Rädel, G.: The Water Vapour Continuum: Brief History and Recent Developments, Surveys in Geophysics, 33, 535–555, doi:10.1007/s10712-011-9170-y, http://link.springer.com/10.1007/s10712-011-9170-y, 2012.

Stamnes, K., Tsay, S.-C., Wiscombe, W., and Jayaweera, K.: Numerically stable algorithm for discrete-ordinate-method radiative transfer in multiple scattering and emitting layered media, Applied Optics, 27, 2502–2509, doi:10.1364/AO.27.002502, http://ao.osa.org/abstract.cfm?URI=ao-27-12-2502, 1988.

Stephens, G. L., Vane, D. G., Boain, R. J., Mace, G. G., Sassen, K., Wang, Z., Illingworth, A. J., O'Connor, E. J., Rossow, W. B., Durden, S. L., Miller, S. D., Austin, R. T., Benedetti, A., Mitrescu, C., and CloudSat Science Team, T.: THE CLOUDSAT MISSION AND THE A-TRAIN: A New Dimension of Space-Based Observations of Clouds and Precipitation, Bulletin of the American Meteorological Society, 83, 1771–1790, doi:10.1175/BAMS-83-12-1771, http://journals.ametsoc.org/doi/abs/10.1175/BAMS-83-12-1771, 2002.

Ström, J., Seifert, M., Kärcher, B., Ovarlez, J., Minikin, A., Gayet, J.-F., Krejci, R., Petzold, A., Auriol, F., Haag, W., Busen, R., Schumann, U., and Hansson, H. C.: Cirrus cloud occurrence as function of ambient relative humidity: a comparison of observations obtained during the INCA experiment, Atmospheric Chemistry and Physics, 3, 1807–1816, doi:10.5194/acp-3-1807-2003, http://www.atmos-chem-phys.net/3/1807/2003/, 2003.

Susskind, J., Barnet, C., and Blaisdell, J.: Retrieval of atmospheric and surface parameters from AIRS/AMSU/HSB data in the presence of clouds, IEEE Transactions on Geoscience and Remote Sensing, 41, 390–409, doi:10.1109/TGRS.2002.808236, http://ieeexplore.ieee.org/lpdocs/epic03/wrapper.htm?arnumber=1196056, 2003.

Turner, D. D. and Löhnert, U.: Information Content and Uncertainties in Thermodynamic Profiles and Liquid Cloud Properties Retrieved from the Ground-Based Atmospheric Emitted Radiance Interferometer (AERI), Journal of Applied Meteorology and Climatology, 53, 752–771, doi:10.1175/JAMC-D-13-0126.1, http://journals.ametsoc.org/doi/abs/10.1175/JAMC-D-13-0126.1, 2014.

Turner, D. D. and Mlawer, E. J.: The Radiative Heating in Underexplored Bands Campaigns, Bulletin of the American Meteorological Society, 91, 911–923, doi:10.1175/2010BAMS2904.1, http://journals.ametsoc.org/doi/abs/10.1175/2010BAMS2904.1, 2010.

Turner, D. D., Merrelli, A., Vimont, D., and Mlawer, E. J.: Impact of modifying the longwave water vapor continuum absorption model on community Earth system model simulations, Journal of Geophysical Research, 117, doi:10.1029/2011JD016440, http://doi.wiley.com/10.1029/2011JD016440, 2012.

Wielicki, B. A., Young, D. F., Mlynczak, M. G., Thome, K. J., Leroy, S., Corliss, J., Anderson, J. G., Ao, C. O., Bantges, R., Best, F., Bowman, K., Brindley, H., Butler, J. J., Collins, W., Dykema, J. A., Doelling, D. R., Feldman, D. R., Fox, N., Huang, X., Holz, R., Huang, Y., Jin, Z., Jennings, D., Johnson, D. G., Jucks, K., Kato, S., Kirk-Davidoff, D. B., Knuteson, R., Kopp, G., Kratz, D. P., Liu, X., Lukashin, C., Mannucci, A. J., Phojanamongkolkij, N., Pilewskie, P., Ramaswamy, V., Revercomb, H., Rice, J., Roberts, Y., Roithmayr, C. M., Rose, F., Sandford, S., Shirley, E. L., Smith, W. L., Soden, B., Speth, P. W., Sun, W., Taylor, P. C., Tobin, D., and Xiong, X.: Achieving Climate Change Absolute Accuracy in Orbit, Bulletin of the American Meteorological Society, 94, 1519–1539, doi:10.1175/BAMS-D-12-00149.1, http://journals.ametsoc.org/doi/abs/10.1175/BAMS-D-12-00149.1, 2013.

Winker, D. M., Pelon, J. R., and McCormick, M. P.: The CALIPSO mission: spaceborne lidar for observation of aerosols and clouds, pp. 1–11, doi:10.1117/12.466539, http://proceedings.spiedigitallibrary.org/proceeding.aspx?articleid=881577, 2003.

Yang, P.: Spectral signature of ice clouds in the far-infrared region: Single-scattering calculations and radiative sensitivity study, Journal of Geophysical Research, 108, doi:10.1029/2002JD003291, http://doi.wiley.com/10.1029/2002JD003291, 2003.

Yang, P., Wei, H., Huang, H.-L., Baum, B. A., Hu, Y. X., Kattawar, G. W., Mishchenko, M. I., and Fu, Q.: Scattering and absorption property database for nonspherical ice particles in the near- through far-infrared spectral region, Applied Optics, 44, 5512, doi:10.1364/AO.44.005512, https://www.osapublishing.org/ao/abstract.cfm?uri=ao-44-26-5512, 2005.